The experimental contact behaviour of natural sands: normal and tangential loading

V. Nardelli* and M.R. Coop[†]

* ONLYgeotechnics Ltd., Hong Kong. Formerly the City University of Hong Kong. Email: vincenzo.nardelli@onlygeotechnics.com

† University College London. Formerly the City University of Hong Kong. Email: m.coop@ucl.ac.uk

ABSTRACT

A comprehensive series of tests were carried out using an innovative three-axis Inter-Particle Loading Apparatus, investigating the normal and shearing contact behaviour between sand particles of a variety of geological origins. The results show that the normal loading behaviour is very sensitive to the type of sand and its surface condition and so its geological origin and history. For particles characterised by a highly regular shape and low surface roughness, such as those of a common quartz sand, good predictions may be made with models based on the elasticity theory, but at lower loads the particle roughness needs to be accounted for. In shearing the coefficient of inter-particle friction is highly variable, both for one sand and between different sands, but the average values are controlled predominantly by the surface roughness. Current elasticity-based methods for predicting the tangential stiffness overestimate it considerably, but coaxiality between the forces and displacements indicate that the underlying assumption of elasticity with micro-slipping at the contacts may be correct.

INTRODUCTION

Owing to the popularity of the Discrete Element Method (DEM), proposed by Cundall & Strack (1979), sands are increasingly being analysed as discrete materials and new approaches have been developed to investigate their mechanical behaviour, both numerically and experimentally. Previously, some micromechanical research had investigated the behaviour of minerals and granular materials using custom-made devices, such as those of Horn & Deere (1962), Skinner (1969) and Procter & Barton (1974), generally with the purpose of relating the angles of inter-particle friction with those of shearing resistance measured at the macro-scale. However, in recent decades, the rôle of micromechanics in geotechnical engineering has expanded, notably to include the effects of particle breakage through single particle crushing tests (McDowell & Bolton, 1998; Nakata et al., 1999; Antonyuk et al., 2005). Only relatively recently has more research concentrated on the contact behaviour (Mullier et al., 1991; Ishibashi et al., 1994; Cole et al., 2010; Cavarretta et al., 2010, 2011). Most of this research has still focussed on the measurement of the coefficient of inter-particle friction, for example Senetakis et al. (2013a) who constructed an initial version of the Inter-Particle Loading Apparatus used here and Cole (2015), who presented an extensive investigation of inter-particle friction and compression behaviour for pairs of particles of a variety of mineralogies, showing very variable results in terms of coefficient of friction. Generally, there has been more work on

load-deflection behaviour prior to breakage in the normal direction (e.g. Cavarretta et al., 2010) than before sliding in the tangential direction (e.g. Cole, 2015). Senetakis et al. (2013b) gave some preliminary data for sliding stiffnesses, although the data were neither extensive enough or repeatable enough to give meaningful comparisons with models commonly used in DEM.

Particle roughness is a key characteristic that may influence the mechanical behaviour of particles, and this has often been measured using an interferometer (e.g. Altuhafi & Coop, 2011). Otsubo et al. (2015) investigated its effect on the elastic stiffness of assemblies of borosilicate ballotini, showing that roughness tended to decrease stiffness but that at higher stress levels the effects of the initial roughness were reduced.

This paper addresses key gaps in the literature for sand contact behaviour. A comprehensive investigation has been made for particles of a variety of origins for both normal and tangential loading, since these are linked in typical models, covering both small and large displacements and making comparisons with those models. This type of data could not be used directly in DEM analyses until other aspects of behaviour, such as shapes, are also correctly modelled, but they should inform on the choice of parameters and also improve our understanding of the relationship between micro and macro-behaviour.

EXPERIMENTAL EQUIPMENT

The contact behaviour of sands was investigated by means of a custom-made Inter-Particle Loading Apparatus, which was originally designed in its 2-D version by Senetakis & Coop (2015), but was upgraded to a 3-D configuration by Nardelli et al. (2016), which was the version used for the experiments presented here. Apart from the capability to load in three orthogonal directions, the apparatus was also stiffened considerably by redesigning some critical parts in order to ensure more accurate stiffness measurements at very small displacements. The introduction of non-contact displacement sensors also minimised the friction of the bearing system, improving the accuracy of the force measurements.

The apparatus (Figure 1) consists of a stiff loading frame (a), with a sled (b) placed on a smooth plate (c) by means of a three-point ball bearing system, and three loading arms. The frame, sled and plate are all made of stainless steel. The redesigned loading arms were 20% stiffer in the vertical direction but about three times stiffer than for the previous 2-D configuration in the horizontal, improving the accuracy of small displacement measurements significantly. The new

stiffness in the horizontal direction was measured at 190 N/mm and in the vertical 1600 N/mm. These stiffnesses were determined by means of tests carried out on either a solid piece of brass or a pair of brass holders glued together using the same super-glue used during the experiments. Both these two test configurations provided similar and repeatable results in terms of stiffness for the vertical and horizontal directions. Also, the friction of the bearing system was determined by means of tests in which the sled was loaded by dead weights, measuring very low values of coefficient of friction (around 0.007-0.01). All the experimental results presented here were corrected for the flexibility of the apparatus and the friction of its bearing system. Further details about the current apparatus configuration and its calibration can be found in Nardelli (2017).

Two sand particles (d) are glued onto brass holders which are connected by means of brass wells to the vertical loading arm and the sled, respectively. The brass holders had a small cylindrical cavity (1mm diameter, 0.2-0.5mm depth) on their top and each particle was pressed into this to minimise the glue thickness at its bottom and to let the glue flow around it, increasing the confinement. Cyanoacrylate super-glue was used and it was cured for at least 24 hours. At the end of the tests, each particle and the glue were removed mechanically. As mentioned above, calibration tests showed that the glue used to attach the particles to the mounts did not contribute significantly to the apparatus flexibility, and so the displacements, once corrected for the apparatus compliance, can be considered to occur only at the particle-particle contact. The whole process was carried out ensuring protection from contamination of the particle surfaces to be tested.

Each loading arm is equipped with a micro-linear actuator (e) and a load cell (f), connected to the sled by means of a pair of orthogonal linear bearings (g). These apply combinations of either forces or displacements along the three directions. The third loading arm was installed to broaden the possible loading combinations, but more importantly it enables measurement of the forces or displacements along the direction orthogonal to that of movement during a typical linear tangential loading test. Previous apparatus, such as the 2-D version of Senetakis & Coop (2014) or the apparatus of Cavarretta et al. (2010), relied on visual observation of the contact surface orientation to ensure that there were no significant out of plane forces, but this was certainly a source of inaccuracy. The non-contact eddy-current displacement sensors (h) have a very high resolution (10^{-5}mm).

The apparatus is in a humidity controlled chamber, which controls the relative humidity within the range 20-85%. The sensor of the humidity controller (i) is shown in Figure 1. Tests under fluid immersed conditions can be carried using a small water bath around the particles. Two micro-cameras (j) help to locate the contact between the particles and record images during testing.

Different kinds of tests can be carried out. The first stage is to apply normal loading, usually at a constant displacement rate, typically between 0.1 and 0.5mm/h. The key output from this stage is the normal load – normal displacement response. Following the application of the normal load, various shear test modes can then be used. The simplest is a tangential loading test, where one particle is sheared linearly over the other at a constant displacement rate (typically 0.02-0.05mm/h) while a constant normal force is applied. Typical outputs of these tests are 1) the tangential load – tangential displacement relationship, from which the degradation curve of tangential stiffness with tangential displacement may be derived, and 2) the coefficient of inter-particle friction μ, which is defined as the ratio between the tangential force and the normal force applied at the contact once the particles are sliding one over the other.

Another type of shear test is termed the "friction test", performed by shearing one particle over the other to failure and then increasing the normal force slowly while continuing to shear, thereby tracing the shearing failure envelope. Finally, more complex 3-D paths can be obtained using both the two horizontal actuators, for example circular paths, which can either be displacement or force controlled. These were performed to investigate the coaxiality between the directions of the forces and displacements. Depending on the type of test, the duration could be anything from two days to a week, including the time required for the sample preparation. The cyclic tests or tests carried out at very low displacement rates tended to be the longer tests. The results of the 163 tests presented in this paper therefore represent a very large body of data. It will be seen later that there is some significant data scatter, but it would not easily be possible to reduce any uncertainty about the data arising from this scatter by carrying out much greater numbers of tests.

MATERIALS TESTED AND EXPERIMENTAL PROCEDURES

Most of the work was carried out on four sands of contrasting origins. These were the Leighton Buzzard sand (LBS), a biogenic carbonate sand (CS), a crushed limestone (LS) and a completely decomposed granite (CDG). Table 1 shows the average chemical compositions of

the materials tested, which were obtained through Energy Dispersive X-ray Spectroscopy (EDS) of the particle surfaces. The roundness and sphericity were determined for each sand by visual observation using the Krumbein & Sloss (1963) chart. For each particle this was done in three orthogonal directions. Mathematical expressions for the calculation of 2-D roundness R and sphericity S were first introduced by Wadell (1932) and Wadell (1933), respectively:

$$R = \frac{\sum_{i=1}^{N} \frac{r_i}{R_0}}{N} \tag{1}$$

$$S = \frac{D}{D_{c\,min}} = \frac{2\sqrt{A/\pi}}{D_{c\,min}} \tag{2}$$

R is obtained as the arithmetic mean of the roundness of the individual corners of the projection on a plane, where the ratio r_i/R_0, with $0<r_i<R_0$, describes the roundness of corner i having a radius r_i, R_0 is the radius of the maximum circle inscribed within the projected outline and N are the number of corners. S can be calculated as the ratio between the diameter D of the area A that is defined by the plane over which the shape parameter is determined and the diameter of the minor circumscribed circle D_{cmin}.

However, it should be emphasised that here the roundness and sphericity were assessed only visually from the Krumbein & Sloss chart and were not calculated from image analysis, which would have been very time consuming and not especially relevant, because, as will be discussed later, the particles were not orientated randomly during the tests but were mounted so as to minimise any influence that the shapes might have on the data. Having also selected particles that had more regular shapes for the tests, again to avoid effects of shape on the data, the values in Table 1 would also not be representative of the whole soil mass but do give an indication of the relative shapes for each type of soil.

The RMS surface roughness S_q of a selected group of particles was measured by means of an interferometer prior to testing them. As reported by Cavarretta (2009), the RMS roughness in 2-D is defined by the expression:

$$S_q = \sqrt{\frac{1}{L} \int_0^L z^2 dx} \tag{3}$$

which represents the root-mean-square deviation of the elevation over the profile $z(x)$ relative to the mean height and where L is the length of the profile. Here 3-D roughnesses were calculated and surface areas of 30x30µm were scanned, which are approximately the same

order of magnitude as typical theoretical contact areas for particles under the normal forces applied during most of the tests (1-5N). Also, using the same scanning areas allowed consistent measurements of roughness to be made for all the materials tested here, since roughness is a dimension dependent parameter, while this relatively small area allowed easier scanning of limestone and CDG that are characterised by a low reflectivity, which makes the measurements more difficult.

The roughness was calculated flattening the images to remove the influence of particle shape. This was done using a default function of the software used to analyse the surface of particles. Ideally, roughness measurements should be made on each of the contacting particles at the location of the contact, but the interferometer tests are far too time consuming and anticipating in advance where the contact will occur too technically difficult to use such an approach for the large number of tests reported here, and so averages are reported from a smaller number of representative particles (Table 2). Particles belonging to Fraction A (2.36-5mm) were generally tested, except for some particle pairs belonging to Fraction B (1.18-2.36mm) for LBS and LS. In each case the same size was used for the upper and lower contacting particles. The size of the particles corresponds to that of the sieve openings that retain them. After selecting the particles, their three principal diameters were determined using a digital calliper with a precision of ±0.01mm. These three values were then used to calculate an average particle diameter for each particle tested, which was also useful for the comparisons with the theoretical models shown in the following sections.

Leighton Buzzard sand (Figs. 2a1-a3) is a sedimentary soil quarried in Southeast England. It is mainly constituted of quartz particles and has been extensively studied worldwide. Todisco (2016) determined an angle of shearing resistance at critical state of 30° for uniformly graded samples. The sand is characterised by grains that have a regular appearance and the particles tested had an average roundness and sphericity of 0.7 and 0.8, respectively. An average RMS roughness of 0.293 ± 0.087μm was measured.

The carbonate sand (Figs. 2b1-b3) has a biogenic origin and was obtained from the Philippines. Its particles originate from the deposition of pieces of coral, foraminifera, bivalve shells and gastropods. Carbonate sands are characterised by brittle and crushable grains, and high angles of shearing resistance at critical state, for example 40° for Dog's Bay sand (Coop & Airy, 2003). This sand is mainly constituted of calcium carbonate, but the EDS analysis showed also a presence of NaCl probably from its marine origin (Table 1). Most of the particles tested were

coral fragments, which are the most abundant fraction, but some tests were also carried out on shell pairs, indicated by the symbol "+". The CS particles had an average roundness and sphericity both equal to 0.7, with different values of sphericity for the coral particles (0.8) and the shells (0.6). The average roughness of the coral fraction was equal to 0.457 ± 0.082mm.

An artificial sand made of crushed limestone rock (Figs. 2c1-c3) was also tested. This material was quarried in Mainland China and was also tested by Todisco (2016) who found an angle of shearing resistance at critical state of 38°, although this was for samples having a fractal grading. This sand consists of pure calcium carbonate and its grains are often very angular and characterised by sharp edges, as they originate from a recent crushing process. For this reason, a low average roundness (0.3) was measured, while the sphericity is higher (0.7). The average roughness of $0.614 \pm 0.341 \mu$m is larger than that of CS, although they have similar mineralogy since the surfaces have been created by breaking.

Finally, a completely decomposed granite (Figs. 2d1-d3) was tested. This sand had its origin from weathering and was retrieved in Hong Kong. As shown in Table 1, its mineralogy reflects the composition of the parent granite, containing quartz, feldspar, and mica as well as clay minerals from the weathering processes. CDG has been previously tested extensively at the macro-scale and values of angles of shearing resistance at critical states between 32° and 38° were determined by Rocchi and Coop (2015) for different weathering degrees. Typically, particles of CDG are constituted of harder grains of quartz and/or feldspar entirely or partially coated by clay minerals (Madhusudhan & Baudet, 2014). For this reason, some particles were washed with water prior to testing (WCDG), in order to remove the clay coating and compare their test results with those for the natural state. The particles are characterised by average values of roundness and sphericity that are medium (0.6) and high (0.8), respectively, while the WCDG has the same sphericity (0.8) but the roundness is much lower (0.3), perhaps related to the sharper edges that are uncovered. The average roughness of CDG is very high ($0.988 \pm 0.303 \mu$m), while lower values were determined for the WCDG particles ($0.429 \pm 0.122 \mu$m).

As reported in Table 2, the main shape and surface characteristics of these four materials were compared with those determined for Eglin sand, ceramic balls and chrome steel balls. Eglin sand is a natural sand characterised by a mixed mineralogy and grains that are generally less regular than the materials described above. The contact response of particle pairs of Eglin sand was previously studied by Nardelli et al. (2017). Also, two artificial sands, ceramic balls and chrome steel balls, were tested as reference materials in order to compare their results with

those obtained for the natural sands. The roundness and sphericity values reported in Table 2 are averages calculated for all the particles tested (around 130 for LBS, 60 for CS, 40 for LS and 20 for natural CDG), while the roughness values were calculated as the mean of those obtained from around 20-30 selected particles for each material.

For the four sands, the SEM images in Figure 2 reflect the surface roughnesses determined using the interferometer. Particles with regular shapes that were also typical of each material were selected, to avoid the influence of shape on the results from especially angular particles, so the shape parameters in Table 2 may not be representative of the whole soil mass, even if significant differences are evident. The mechanical properties of the materials are reported in Table 3. These include the Young's modulus E, the shear modulus G and the Poisson's ratio v of the main mineral constituting the particles along with their microhardness and the indentation modulus determined from microhardness or nanohardness tests, as indicated. The hardness of a material is the resistance, which has the dimensions of stress, to the penetration (i.e. an applied displacement) of an indenter. This can be a micro or nano-indenter for small scale hardness measurements. The microhardness values were determined through tests on real sand particles from the fraction 2.36-5mm by means of a device that follows the Vickers standard. These moduli represent useful information for the description of the mechanical response of rough surfaces in contact and are compared with those for chrome steel balls in Table 3.

EXPERIMENTAL RESULTS

Most of the test results were obtained from normal and simple tangential loading tests. The particles were sheared on selected convex apex-apex contacts and generally only very short shear paths were necessary to reach a steady state value of the tangential force. For this reason, the results were not significantly influenced by the particle shape parameters in Table 2. The small displacements also mean that the vertical and horizontal forces measured during the tests could be considered as normal and tangential, avoiding the need to resolve them, as Cavarretta et al. (2010) had to do for their longer shearing paths. This was confirmed analysing the vertical displacements during the shear tests. Figure 3 gives three examples, showing the evolution of the vertical displacements with the horizontal displacements during shear tests performed on particle pairs of LBS and coral and shell particles of CS, each confined under 1N. The particle pairs were sheared forward and backwards and it can be observed that vertical displacements for the shell particles and LBS are very small, in the case of LBS equal to 3.5% of the maximum

horizontal displacement of 0.01mm, which was enough to reach the steady state. For the coral particles, compressive vertical displacements can be observed while the particles are both sheared forward and backwards. This cannot be related to shape because if it had been it would have been 1) reversible and 2) not always compressive. It is therefore probably related to the damage arising from the low microhardness of the particle surfaces, which makes them very soft during shearing, so it is difficult to recognise any effect of shape on their mechanical response. Also, particles of LS and CDG exhibited a behaviour similar to this.

The tangential stiffnesses were calculated as tangents to the force-displacement curves taken by regression over a number of data points. These have the dimension of force over displacement (N/mm). The main information of the shear tests carried out for each soil type (i.e., number of tests, range of confining force and displacement rate range) is included in Table 4. Prior to performing any shear test on a pair of particles, a normal loading test was carried out in order to study the compressive contact response of the grains. Hence, the same total number of compression and shear tests was performed.

Normal loading

Figures 4 and 5 show normal loading test data for water immersed LBS, CS and LS up to 1 and 10N, respectively. The tests for the LBS show typical Hertzian type non-linear force-displacement relationships and consistent slopes between different tests, especially at higher loads, following initial displacements that are very limited and much smaller than those observed by Cavarretta et al. (2010). The CS and LS particles exhibit a contact response that is much more variable, sometimes with a more significant initial offset. It is possible that for these more irregular particles, such as the LS, the variability of local contact geometry, which was not measured, may add to the data scatter. These soils are also sometimes characterised by brittle behaviour and force-displacement curves that are not smooth, possibly related to the crushing of asperities. This occurs for the coral particles of CS at very low loads (lower than 1N), while it takes place for LS more frequently at loads that are higher, perhaps because it is influenced by the greater hardness of the LS, even though they are both constituted of calcium carbonate (Table 3). Apart from these artefacts, again probably due to damage, no clear example of yield at higher normal loads was seen, as had been suggested by Antonyuk et al. (2005) for industrial granulates. The shell particle pairs of CS (+) exhibit a very stiff contact response, which is comparable to that of LBS and which is very different from that of the coral

fragments, which is probably related to a different surface microstructure of the two types of CS.

A comparison between four tests each for CDG and WCDG up to a maximum load of 10N is reported in Figure 6. These were carried out at a relative humidity of 85% rather than immersed, to preserve the difference between the washed and unwashed particles. The contact response of the washed WCDG particles is stiffer and more consistent than that of unwashed CDG, since it is not affected by the clay coating. The thickness of this film was observed to be variable and this leads to normal contact stiffnesses that can also be quite variable. The CDG is characterised by a ductile response that is much softer than that of the other materials probably arising from the clay coating, which deforms but does not crush as may occur to asperities on CS and LS particles.

Another comparison up to very high normal forces is illustrated in Figure 7. Here the results of cyclic normal tests on LBS up to 31N and WCDG up to 30N are illustrated along with those for a load-unload-reload test on a CDG particle pair up to 25N. A completely different magnitude of displacements during first loading can be observed for CDG, with large plastic displacements after the first unloading path. On the other hand, WCDG exhibits a contact response that is much stiffer and mainly reversible, but still with plastic displacements of around 10μm after the first unloading. The slope of the force-displacement curve of WCDG is quite similar to that of LBS, showing that the contact behaviour of this material is related to that of the stiff minerals (either quartz or feldspar) that can be found within the particles, without the effect of the clay coating. Also, it can be observed that the normal contact behaviour of a stiff natural sand such as LBS is mostly reversible and its slope is steeper than that of a relatively young and weathered surface, such as that of CDG or a young and fresh broken surface like the LS.

Monotonic tangential loading

The results of six tangential loading tests on LBS under water immersed conditions and different normal loads between 1 and 20N are illustrated in terms of force-displacement and stiffness-displacement in Figure 8a and b, respectively. The force-displacement curves show a typical non-linear response in the initial stages of shearing, with a gradual decrease of the slope until a steady state value of tangential force is reached at particle sliding. Even if the initial stiffness increases with normal load, the steady state is reached at larger displacements. For

these few tests on different particles the data are quite scattered and so, while there is clearly a rôle of the normal load on the tangential stiffness, the data are not always consistent.

Figures 9 and 10 show similar tangential loading tests on CS and LS. For these materials the force-displacement curves are less smooth and sometimes sudden drops of tangential force occurred, probably related to a brittle behaviour at the contact. The behaviour of shell particles of CS is usually stiffer than that of coral, although these also usually exhibit a fragile behaviour. For both CS and LS the stiffnesses show a clear increase for increasing normal loads. Also, it can be observed that the initial stiffness of LS is clearly lower than that of CS although these sands have similar mineralogies.

Three tangential loading tests each on CDG and WCDG particles are reported in Figure 11. Surprisingly, the results show similar force-displacement curves, while the WCDG exhibits a contact behaviour that seems more brittle than that of CDG, perhaps related to the effect of the clay coating that might increase the ductility. The tangential stiffnesses of these particles seem to increase for higher confining loads, although this is not as clear as observed for CS or LS.

Cyclic tangential loading

Figure 12 shows a cyclic test on LBS particles submerged in distilled water, in which four displacement controlled cycles of ±1μm were carried out under a normal load of 3N. The particles were sheared within this displacement range in order not to reach sliding failure. The force-displacement curves show a contact behaviour that is predominately reversible although small hysteresis loops can be observed for each cycle. The tangential stiffness seems unaffected by this small number of cycles, with a similar trend of degradation for each cycle in Figure 12b. This non-linear, largely elastic but hysteretic behaviour is what is expected from the Mindlin & Deresiewicz (1953) model, for which the contact behaviour is essentially elastic, but non-linearity occurs due to micro-slipping at the contact.

A cyclic test on CS coral fragments is shown in Figure 13. In this case, three displacement-controlled cycles of ±0.8μm were carried out under a normal load of 3N. Also for CS a substantially reversible behaviour can be observed, showing small hysteresis loops in the force-displacement plots and similar values of initial stiffness for each cycle.

Circular shearing paths

The LBS contact behaviour was also studied through circular loading tests. These were carried out on this particular sand since its grains are generally more regular than those of other materials and this minimises the effects of the shape on the test results. This type of test was performed both in order to obtain data for very large displacements, while shearing the particles continuously along a circular path, and study the coaxiality between force and displacement vectors during the tests, while applying either circular displacement or force paths at the particle contacts. Figure 14 shows the displacement paths along the two horizontal directions H1 and H2 along with the force increment vectors plotted on the path for the first (a) and the twelfth cycle (b). The radius of the shearing path is 0.1mm, the vertical load was 3N and shearing was at a rate of one cycle per hour. At these large displacements the steady state is continuously maintained and so the force and displacement directions coincide, as they should for frictional sliding.

More interesting is the force-controlled circular test in Figure 15, where the particles were sheared at forces that are lower than those at steady state, to investigate the nature of the mechanical response before sliding. In Figure 15 the radius of the path is 0.6N and the particles were under a normal load of 4N. The plastic displacement increment vectors were calculated and plotted along the shear path. These were calculated as resultants from the displacements measured during the circular shear, deducting the elastic component of the displacement estimated from the tangential loading tests carried out at the same confining force. The graph shows that the plastic displacement increment vectors are generally almost coaxial with the direction of the force path, with a few exceptions that may result from artefacts of the surface topology. This tends to confirm the Mindlin & Deresiewicz hypothesis that the non-linearity of tangential response results from micro-slipping at the contact. Any true plasticity at the contact surface might have been reflected by non-coaxiality.

Rate effects in shearing

A brief investigation of the tangential loading behaviour of sand particles sheared at different displacement rates was carried out on LBS. Figure 16 shows a test where the particles were confined under a normal load of 3N and sheared at displacement rates successively of 0.02mm/h, 0.2mm/h and 0.003mm/h. The force-displacement curves show that similar values of tangential force at steady state are reached for the displacement rates of 0.02 and 0.003mm/h where angles of inter-particle friction coefficient of 0.20 are measured, while values slightly

higher (0.22) are measured in the initial path for the rate of 0.2mm/h, but this drops towards similar values to the slower rates at larger displacements. The stiffnesses of the three different paths also seem unaffected by the different test rates. In DEM analyses, creep has been modelled by using a coefficient of friction that increases with velocity when the rates of shearing are very small (Kuhn & Mitchell, 1993; Kwok & Bolton, 2010). This is based on experimental evidence from, for example, Burwell & Rabinowicz (1953) who sheared steel on a very soft metal (Indium), there being no data for soils. However, from these data, for the speeds of shearing used here the coefficient of friction should be increasing by over 10% per log cycle of speed, which it clearly does not.

Effect of the loading history

Figures 17 and 18 show tests investigating the effect of the loading history on the contact behaviour of LBS and CS, respectively. As shown in Figure 17, two tests were carried out on the same LBS particles, which were sheared after initially applying a normal load of 1N (LBS31), then, after returning the contact to the same initial position, the normal load was increased up to 30N and then reduced back to 1N before a second tangential loading test was carried out on the previously loaded contact (LBS32). This procedure is comparable to that of "overconsolidation" of soils, but this phenomenon occurs only locally, in a small portion of the particles tested that is close to their contact. The stiffness at very small displacements increased after this process, but the value of inter-particle friction (0.18) did not, so that smaller displacements were required to reach the steady state condition after the "overconsolidation". Some stick-slip behaviour observed during the first test is not seen in the second.

For the CS particles (Fig. 18), after "overconsolidation" to 10N both the steady state friction and the stiffness at larger displacements are increased, although the stiffness at the smallest displacements is not much affected. Possibly, some damage may have occurred at the contact between the CS particles because of their softer nature than the LBS, leading to an increase of surface roughness, but unfortunately it was not possible to make a measurement of this.

Effect of the environmental conditions

Figure 19 shows the failure envelopes for LBS (a), CS (b) and LS (c), for the different conditions of low humidity (LH, relative humidity RH<30%), high humidity (HH, RH>80%) and water immersed conditions (W). The different environmental conditions were applied for 2-3 hours before carrying out each test. The data scatter is large and so the very small

differences between each of the failure envelopes are not significant. The slightly lower value of inter-particle friction coefficient μ for immersed LS particles was affected by crushing and brittle behaviour at the contacts. These data therefore indicate that water has little effect on inter-particle friction for sands, in contrast to the results of Skinner (1969).

Failure envelopes and inter-particle friction

To study the effect of normal load on the failure envelopes, "friction" tests were carried out on LBS. Figure 20 shows tests where the normal load was increased within the range 1-12N while shearing the particles, along with the data points representing the maximum tangential load during the simple tangential loading tests for normal loads up to 10N. Within the scatter the two types of test give similar values of friction, but the friction test paths generally exhibit a clear curvature. Normal loads were investigated for LBS up to 50N, since these particles are stronger than the other sands and, because of this curvature, the friction coefficient depends on the load range considered (Figure 21), with 0.20 for 0-10N and 0.17 for 0-50N. Figure 22 shows the failure envelopes of CDG and WCDG for normal loads up to 10N. These show that μ for the natural particles and those for the washed particles have similar values (0.35), despite the clay coating on the natural CDG.

The failure envelopes for all four sands along with that of Eglin sand and chrome steel balls (ST) are reported in Figure 23. The Eglin sand data were reported elsewhere (Nardelli et al., 2017), since this has a complex mineralogy and so is not easily compared in detail with the others. Only the results from tangential loading tests where the particles were sheared once are included. All the sands exhibit coefficients of friction that are much higher than that for an artificial material such as ST, while CS and LS have very different values despite their similar mineralogy. This is related to the fact that for the LS brittle behaviour, possibly due to damage, generally occurred while the shear stress was still increasing and before a steady state was reached.

It can be observed that μ is possibly lower for those materials characterised by high elastic moduli and surface hardness. Also, the coefficient of inter-particle friction seems affected by the surface roughness (Figure 24). In this figure, the results from the different Eglin sand minerals that are identified by their colour (Nardelli et al., 2017) along with those for ST and also some ceramic balls (CB) (Nardelli, 2017) are included. An increasing trend of μ with roughness can be clearly identified. This effect of roughness is therefore the cause of some of

the scatter of individual data points for each sand since it was impractical to measure the roughness of both sides of every contact pair.

Figure 25 shows a plot of the average particle regularity (Cho et al., 2006), which describes the particle shape as the mean of roundness and sphericity, against the coefficient of inter-particle friction for all the materials tested. It can be observed that the relationship is not very clear, especially among the natural particles. Superficially it might be claimed that there is a rough trend of decreasing μ with increasing regularity, until it is recalled that 1) what is plotted is the overall shapes of the particles but that the particle pairs were actually orientated selectively to minimise shape effects, and 2) the vertical displacements measured during shearing confirmed that there were no shape effects. It should in any case be expected that the friction coefficient could only be affected by particle surface features within the size of the contact. This is the size used for the roughness measurements and while the images were flattened prior to quantifying roughness, this routine selects a smoothed surface that would be unlikely to eliminate features that might affect friction but would not be measured by the vertical displacement during the test.

The key comparison which argues against any clear effect of shape is that between the two most regular natural particles, the LBS and the carbonate sand. Even if these have the same regularity, the value of μ is very much lower for the LBS. A possible explanation for any slight trend with shape is that the natural processes occurring during the creation of the soil that tend to make it smoother or rougher also might tend to affect the shape, so that some have described the morphology of sand particles using fractals (Yang et al., 2016). If the scatter of data that is evident in the relationship between μ and roughness is not due to shape effects, it could well arise from the effects of damage to the surfaces of softer particles.

COMPARISONS WITH THEORETICAL MODELS

The experimental results were compared with those predicted using some common models in contact mechanics for normal and tangential loading. These are the Hertz (1882) and the Mindlin & Deresiewicz (1953) models, respectively, both determined for materials other than soils. For normal loading, a modified Hertz model proposed by Greenwood et al. (1984) was also adopted to include the effect of surface roughness. The symbol "*" is used to identify the curves obtained using this model. The relative radii, which is a value that accounts for the

different individual radii of the particles and are necessary for the calculations, were determined directly from the particles. The comparisons between experimental results and the theoretical predictions presented here assume that the contact behaviour of particles is influenced by the average geometrical measurements of the particles, where each of them was modelled as a sphere having a diameter which is the average of those measured. The comparisons focus on the LBS and coral fraction of CS since these are single mineral soils of more regular shape.

Normal loading

Figure 26 shows examples of comparisons between normal loading tests on LBS and CS and predictions using the Hertz theory and the modified Hertz model including particle roughness, up to a normal load of 1N. The approach taken was to fit the data by varying the Young's modulus used and then compare the values derived with published data (Table 3). For these low load levels, the modified Hertz model seems to fit the data well using Young's moduli (94GPa and 68GPa for LBS and CS) that are similar to the values found in the literature for quartz and calcite, while the values of E needed to obtain a good fit with the classical Hertz model are unreasonably low. This is possibly because the asperities of the particle surface are unlikely to be completely deformed at these low load levels. The theoretical curves plotted for CS started with an offset of 0.6μm, since the Hertz model seems unable to fit the initial very soft behaviour for this soil.

For larger normal loads higher elastic moduli are required for both models to fit the experimental data (Fig. 27) so that including roughness could not provide a good fit using reasonable values of E, while the classical Hertz theory provides a good prediction with material parameters similar to those in the literature (E=110GPa and 77GPa for LBS and CS). It is possible that at these higher loads the asperities have become flattened and no longer influence the behaviour. Also in this case, the theoretical curves for CS were plotted with an initial offset (3.4μm), which is significantly higher than the sum of the heights of the asperities of the two particles in contact using average values for CS. This is probably related to the soft surface of this material, which appears softer than the bulk as is confirmed by the low values of microhardness and indentation modulus measured for CS, which are considerably lower than those determined for LBS despite the Young's moduli of these two materials have similar magnitude (Table 3).

Tangential loading

A comparison between a tangential loading test on LBS with 7N vertical load and the Mindlin & Deresiewicz contact model is shown in Figure 28. Two theoretical curves are plotted, one where the initial stiffness was calculated by means of the Young's modulus of quartz (taken as 94GPa) and another where the actual initial stiffness determined from the test was used. The theoretical curve shows a behaviour that is stiffer than that determined experimentally, but a good fit can be obtained using the experimental initial stiffness. This indicates that while the initial stiffness calculated by means of the model is not very precise, the empirical decay rule it uses is reasonable.

On Figure 28 the differences of measured and calculated stiffnesses seem not large, but Figure 29 shows more clearly that they are actually very significant. The experimental and theoretical values are shown for displacements of 0.1 and 1μm. Two pairs of theoretical predictions are plotted, using the minimum and the maximum diameters of the LBS particles (D_{min}=1.18mm and D_{max}=3.5mm). A Young's modulus of 94GPa, a Poisson's ratio of 0.065 and a coefficient of inter-particle friction equal to 0.19 were used for the theoretical predictions. While the theoretical values are much higher at both displacement levels, the general trend is similar to the data with an increase of stiffness for larger normal loads. For the CS particles (Figure 30) the mechanical parameters of calcite were used with a μ of 0.4, but the discrepancy between data and theory is even greater, possibly again due to the softer nature of the contact. It is also possible that the local contact geometry adds to the scatter of the data in both normal and shear loading, but it would require X-ray CT to quantify the contact geometry accurately. This would not, however, alter the conclusion that the measured behaviour in shear is very much softer than that predicted.

CONCLUSIONS

The results presented showed the potential of the 3-D version of the Inter-Particle Loading Apparatus to investigate many aspects of the contact behaviour of sands at the micro-scale. In normal loading the data for a quartz sand (LBS) are relatively consistent and stiff while those for rougher new broken rock surfaces (LS) or where there is a weathered surface (CDG) are softer and much more variable. Comparisons with theoretical predictions based on the theory of elasticity indicate that where the data are more consistent good predictions may be made and

that the surface roughness does affect the contact stiffness at smaller loads but not at larger. However, for a softer material like the carbonate sand there were some small initial offsets of displacement that could not be accounted for.

In shear loading the coefficients of friction were highly variable, even for one sand type, since these were strongly related to surface roughness. The mean values of inter-particle friction, which vary almost by a factor of two between the sands, appear therefore to be more variable than the tangents of the critical state angles of shearing resistance would be. The observed tangential stiffnesses were much softer than those predicted from the elasticity theory, but the rate of decay was similar to that assumed by such models. The tests were designed to minimise the effects of shape on the contact behaviour and no clear effect could be seen in the friction coefficient, although local shape at the contact might add to the scatter of the stiffness data.

The behaviour prior to sliding was elastic and hysteretic as the theory predicts and the force and displacement vectors were coaxial for the harder LBS, indicating no significant plasticity, so that the non-linearity and permanent displacements may well result from micro-slippage as suggested by the theory. Rate effects were found not to be significant over nearly two orders of magnitude of velocity, but a heavy normal pre-loading of a contact can change its shearing behaviour in softer materials.

ACKNOWLEDGEMENTS

REFERENCES

Altuhafi, F.N. & Coop, M.R. (2011). Changes to particle characteristics associated with the compression of sands. Géotechnique, 61(6), 459-471.

Antonyuk, S., Tomas, J., Heinrich, S. & Mörl, L. (2005). Breakage behaviour of spherical granulates by compression. Chem. Eng. Sc., 60(14), 4031-4044.

Broz, M.E., Cook. R.F & Whitney, D.L. (2006). Microhardness, toughness and modulus of Mohs scale minerals. American Mineralogist, 91(1), 135-142.

Burwell, J.T. & Rabinowicz, E. (1953). The nature of the coefficient of friction. J. Appl. Phys., 24(2), 136-139.

Cavarretta, I., (2009). The influence of particle characteristics on the engineering behaviour of granular materials. PhD thesis, Imperial College, London.

Cavarretta, I., Coop, M.R. & O'Sullivan, C. (2010). The influence of particle characteristics on the behaviour of coarse grained soils. Géotechnique 60(6), 413-423.

Cavarretta, I., Rocchi, I. & Coop, M.R. (2011). A new inter-particle friction apparatus for granular materials. Can. Geotech. J., 48(12), 1829-1840.

Cho, G.C., Dodds, J. & Santamarina, C. (2006). Particle Shape Effects on Packing Density, Stiffness, and Strength: Natural and Crushed Sands. Journal of Geotechnical and Geoenvironmental Engineering, ASCE, 132, No. 5, 591-602.

Cole, D.M. (2015). Laboratory observations of frictional sliding of individual contacts in geologic materials. Granular Matter, 17(1), 95-110.

Cole, D.M., Mathisen, L.U., Hopkins, M.A. & Knapp, B.R. (2010). Normal and sliding contact experiments on gneiss. Granular Matter, 12(1), 69–86.

Coop, M.R. & Airey, D.W. (2003). Carbonate sands. Characterisation and engineering properties of natural soils, T.S. Tan, K.K. Phoon, D.W. Hight, and S. Leroueil, eds., A.A. Balkema Publishers, 1049-1086.

Cundall, P.A. & Strack, O.D.L (1979). A discrete numerical model for granular assemblies. Géotechnique, 29(1), 47–65.

Greenwood, J.A., Johnson, K.L. & Matsubara, E. (1984). A surface roughness parameter in Hertz contact. Wear, 100, 47-57.

Hertz, H. (1882). Über die Berührung fester elastischer Körper. J. Reine und Angewandte Mathematik, 92, 156-171.

Horn, H.M. & Deere, M.S. (1962). Frictional characteristics of minerals. Géotechnique, 12(4), 319-335.

Ishibashi, I., Perry, C. & Agarwal, T.C. (1994). Experimental investigations of contact friction for spherical glass particles. Soils & Foundations, 43(4), 79-84.

Jaeger, J.C., Cook, N.G.W. & Zimmerman, R. (2007). Fundamentals of rock mechanics. Fourth edition. Wiley-Blackwell.

Krumbein, W.C. & Sloss. L.L. (1963). *Stratigraphy and Sedimentation*. San Francisco, W. H. Freeman and Company.

Kuhn, M.R. & Mitchell, J.K. (1993). New perspectives on soil creep. ASCE J. Geotech. Engng 119(3), 507-524.

Kwok, C. Y. & Bolton, M.D. (2010). DEM simulations of thermally activated creep in soils. Géotechnique, 60(6), 425-433.

Madhusudhan, B.N. & Baudet, B.A. (2014). Influence of reconstitution method on the behaviour of completely decomposed granite. Géotechnique, 64(7), 540-550.

Mavko, G., Mukerji, T. & Dvorkin, J. (1998). *The rock physics handbook: tools for seismic analysis in porous media*. Cambridge University Press.

McDowell, G.R. & Bolton, M.D. (1998). On the micromechanics of crushable aggregates. Géotechnique, 48(5) 667–679.

Mindlin, R.D. & Deresiewicz, H. (1953). Elastic Spheres in Contact Under Varying Oblique Forces. J. Appl. Phys., 327-343.

Mullier, M., Tuzun, U. & Walton, O.R. (1991). A single-particle friction cell for measuring contact frictional properties of granular materials. Powder Technology, 65(1-3), 61-74.

Nakata, Y., Hyde, A.F.L., Hyodo, M. & Murata, H. (1999). A probabilistic approach to sand crushing in the triaxial test. Géotechnique, 49(5), 567-583.

Nardelli, V. (2017). An Experimental Investigation of the Micromechanical Contact Behaviour of Soils. PhD Thesis, City University of Hong Kong.

Nardelli, V., Coop, M.R., Andrade, J.E. & Paccagnella, F. (2017). An experimental investigation of the micromechanics of Eglin sand. Powder Technology, 312, 166-174.

Nardelli, V., Coop, M.R., Vitone, C. & Chen, S. (2016). The inter-scale behaviour of two natural scaly clays. Géotechnique Letters, 6(3), 205-210.

Oliver, W.C. & Pharr G.M. (1992). An improved technique for determining hardness and elastic modulus using load and displacement sensing indentation experiments. J. Mats Res., 7(6), 1564-1583.

Otsubo, M., O'Sullivan, C., Sim, W.W. & Ibraim, E. (2015). Quantitative assessment of the influence of surface roughness on soil stiffness. Géotechnique, 65(8), 694-700.

Procter, D.C. & Barton R.R. (1974). Measurements of the angle of interparticle friction. Géotechnique, 24(4), 581-604.

Rocchi, I. & Coop, M.R. (2015). The effects of weathering on the physical and mechanical properties of a granitic saprolite. Géotechnique, 65(6), 482-493.

Senetakis, K. & Coop, M.R. (2014). The development of a new micro-mechanical inter-particle loading apparatus. Geotech. Testing J., 37(6), 1028-1039.

Senetakis, K., Coop, M.R. & Todisco. M.C. (2013a). The inter-particle coefficient of friction at the contacts of Leighton Buzzard sand quartz minerals. Soils & Foundations, 53(5), 746-755.

Senetakis, K., Coop, M.R. & Todisco. M.C. (2013b). Tangential load-deflection behaviour at the contacts of soil particles. Géotechnique Letters, 3(2), 59-66.

Skinner, A.E. (1969). A note on the influence of interparticle friction on shearing strength of a random assembly of spherical particles. Géotechnique, 19(1), 150-157.

Todisco, M.C. (2016). Behaviour of non-convergent soils: effect of particle size, mineralogy and fabric. PhD Thesis. City University of Hong Kong.

Todisco, M.C., Wang, W., Coop, M.R. & Senetakis, K. (2017). Multiple contact compression tests in particles crushing. Soils & Foundations, 57(1), 126-140.

Wadell, H. (1932). Volume, shape, and roundness of rock particles. Journal of Geology, 40, 443-451.

Wadell, H. (1933). Sphericity and roundness of rock particles. Journal of Geology, 41, 310-330.

Yang, H., Baudet, B. A. & Yao, T. (2016). Characterization of the surface roughness of sand particles using an advanced fractal approach. Proc. R. Soc. A 472: 20160524. http://dx.doi.org/10.1098/rspa.2016.0524

NOMENCLATURE

CB	Ceramic balls
CDG	Completely decomposed granite
CS	Carbonate sand
D	Particle diameter
E	Young's modulus
ES	Eglin sand
G	Shear modulus
LS	Crushed limestone sand
LBS	Leighton Buzzard sand
R	Roundness
RH	Relative humidity
ST	Chrome steel balls
S	Sphericity
S_q	RMS roughness
WCDG	Washed completely decomposed granite
μ	coefficient of inter-particle friction
ν	Poisson's ratio
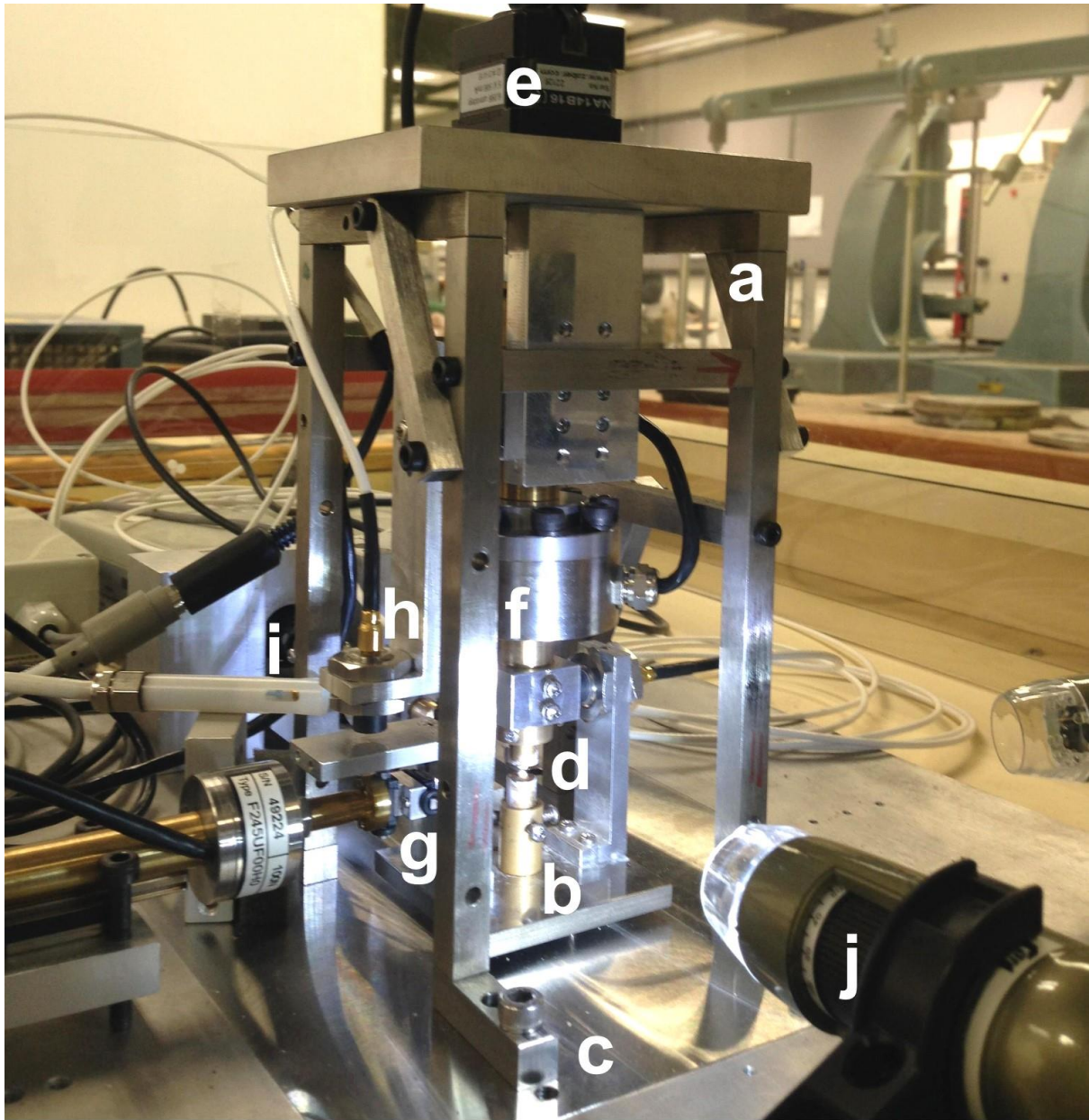
Fig. 1. The Inter-Particle Loading Apparatus: a) loading frame; b) stainless steel sled; c) smooth steel plate; d) particles during a test; e) micro-linear actuator; f) load cell; h) eddy-current displacement sensor; i) humidity sensor; l) digital micro-camera.
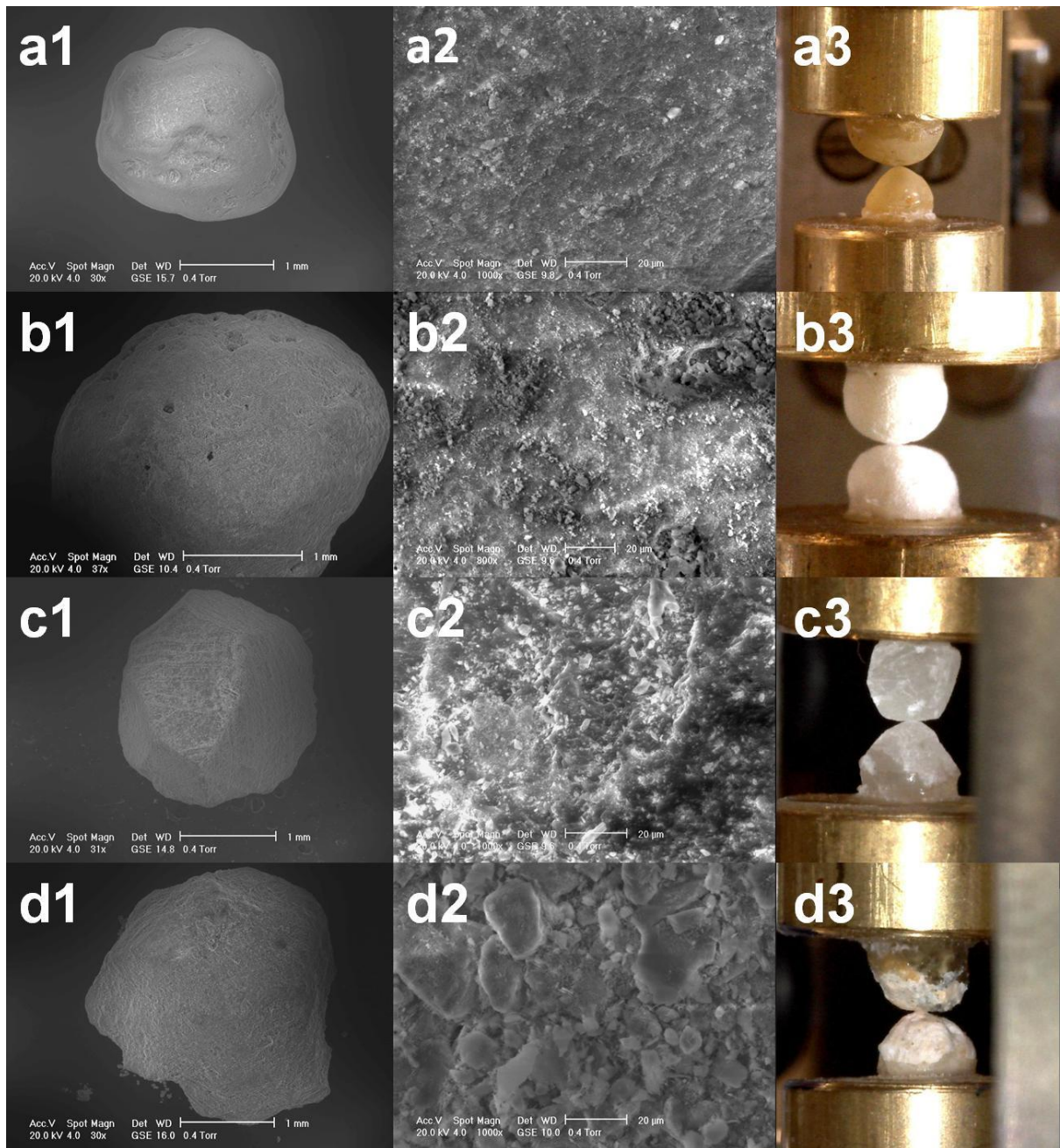
Fig. 2. SEM images and test pictures of the materials tested: a1-3) Leighton Buzzard sand, b1-3) carbonate sand, c1-3) limestone; d1-3) completely decomposed granite (a2-d2, magnification 1000x, except 800x for CS).
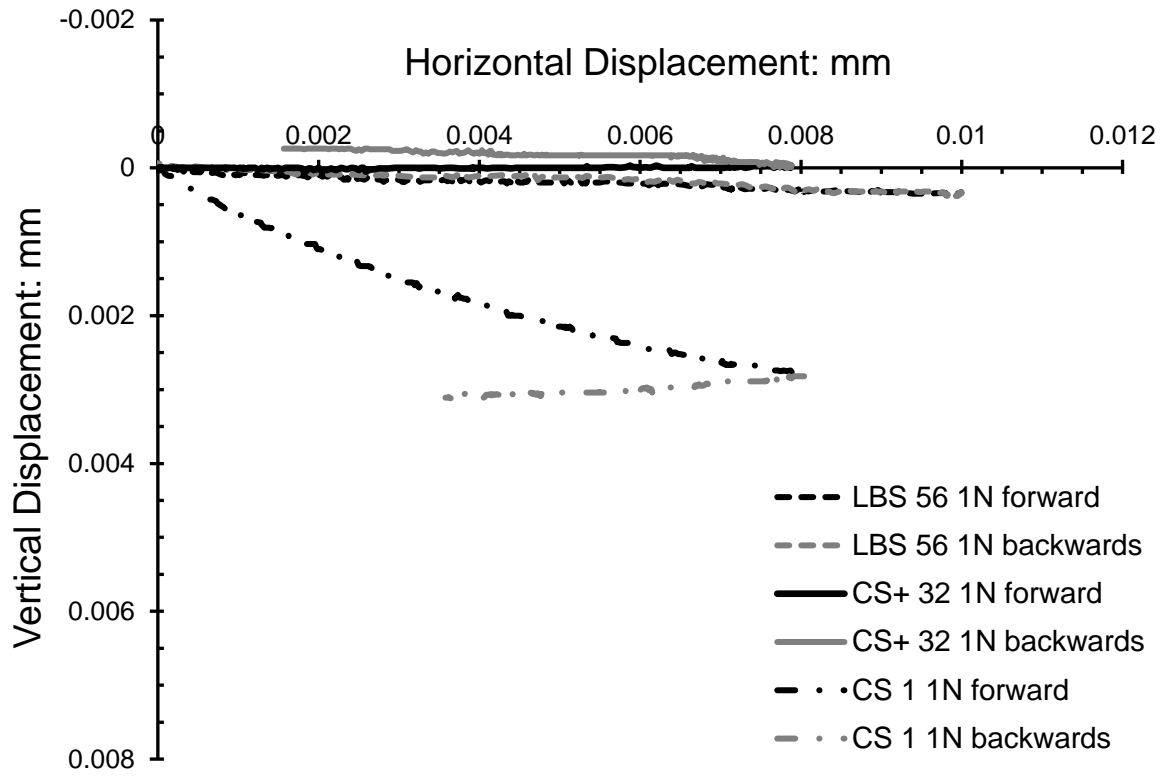
Fig. 3. Vertical displacements-horizontal displacement plots for shear tests on LBS and coral and shell particle pairs of CS confined under 1N.
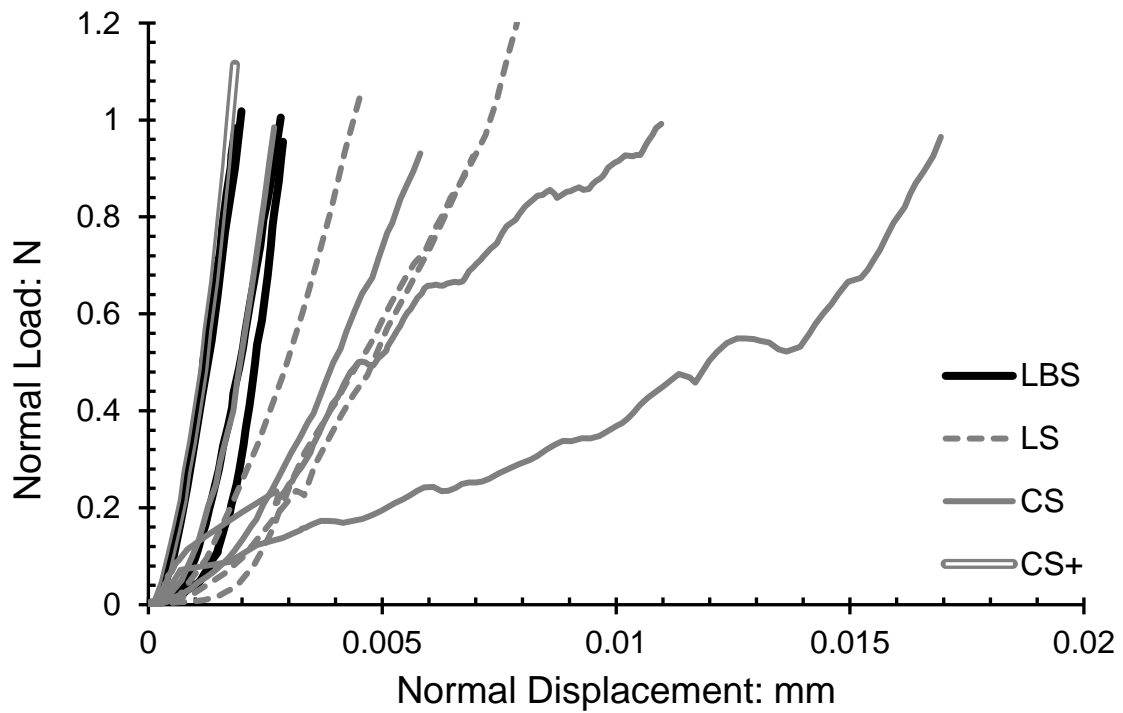
Fig. 4. Normal loading test results for LBS, CS and LS up to 1N.
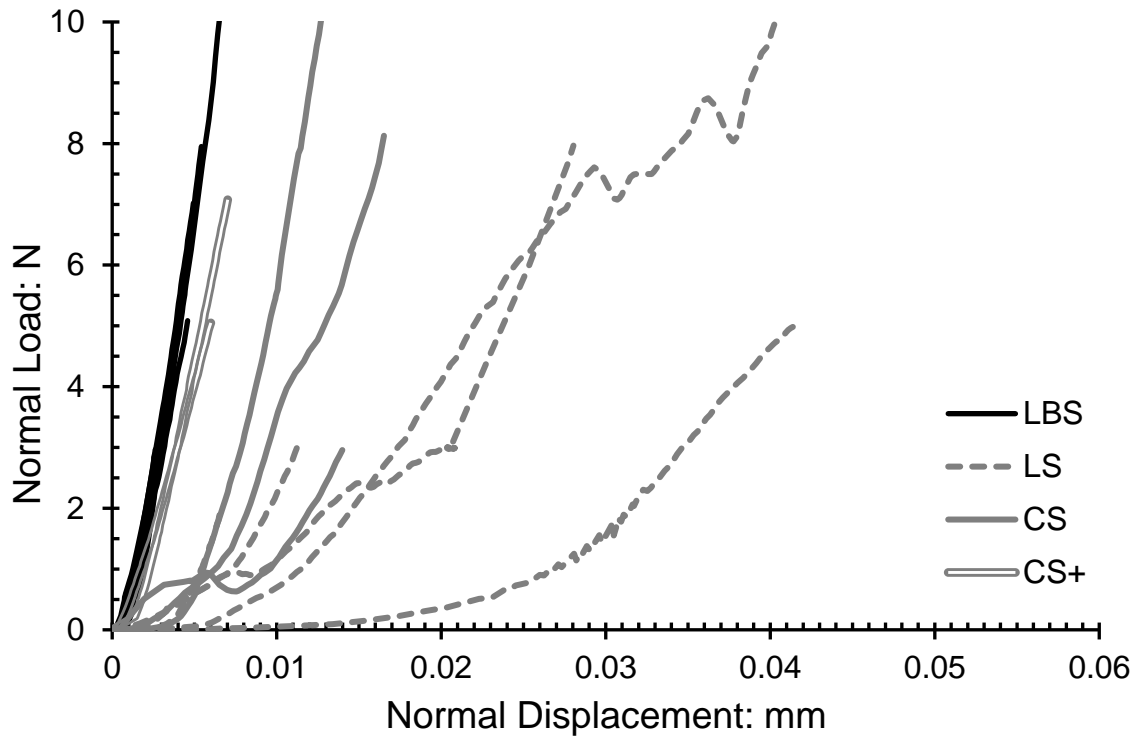
Fig. 5. Normal loading test results for LBS, CS and LS up to 10N.
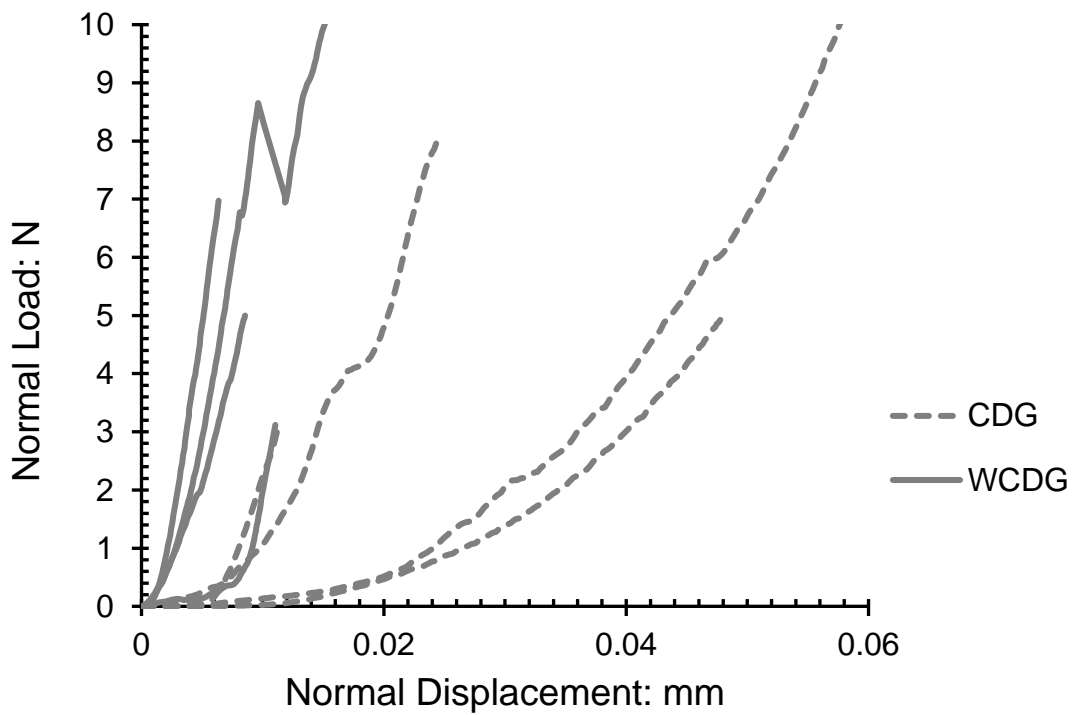
Fig. 6. Normal loading test results for CDG and WCDG up to 10N.
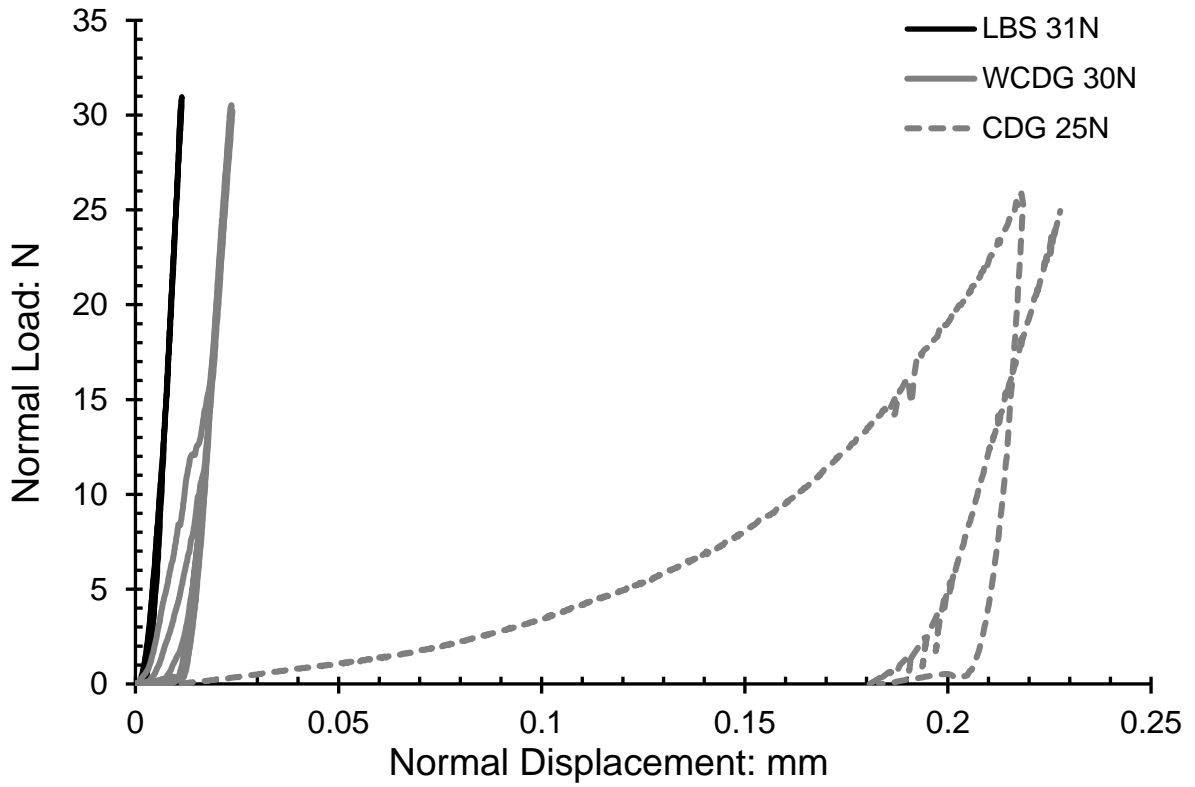
Fig. 7. Cyclic normal loading test results for LBS, CDG and WCDG up to higher forces (25-31N).
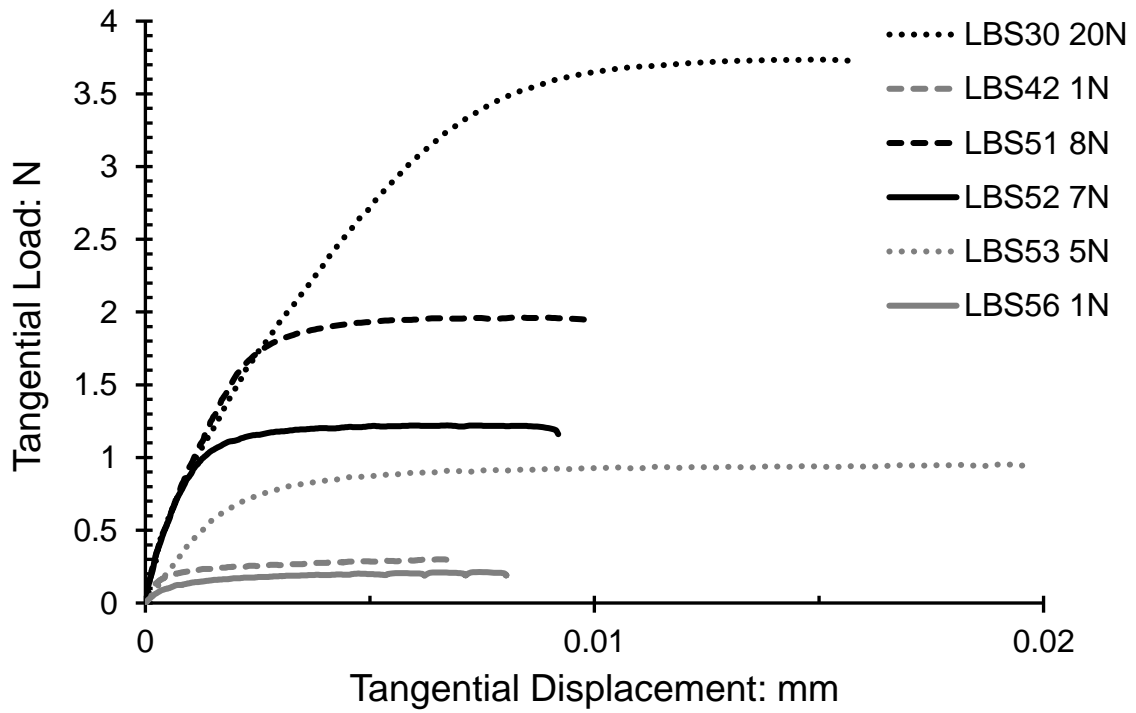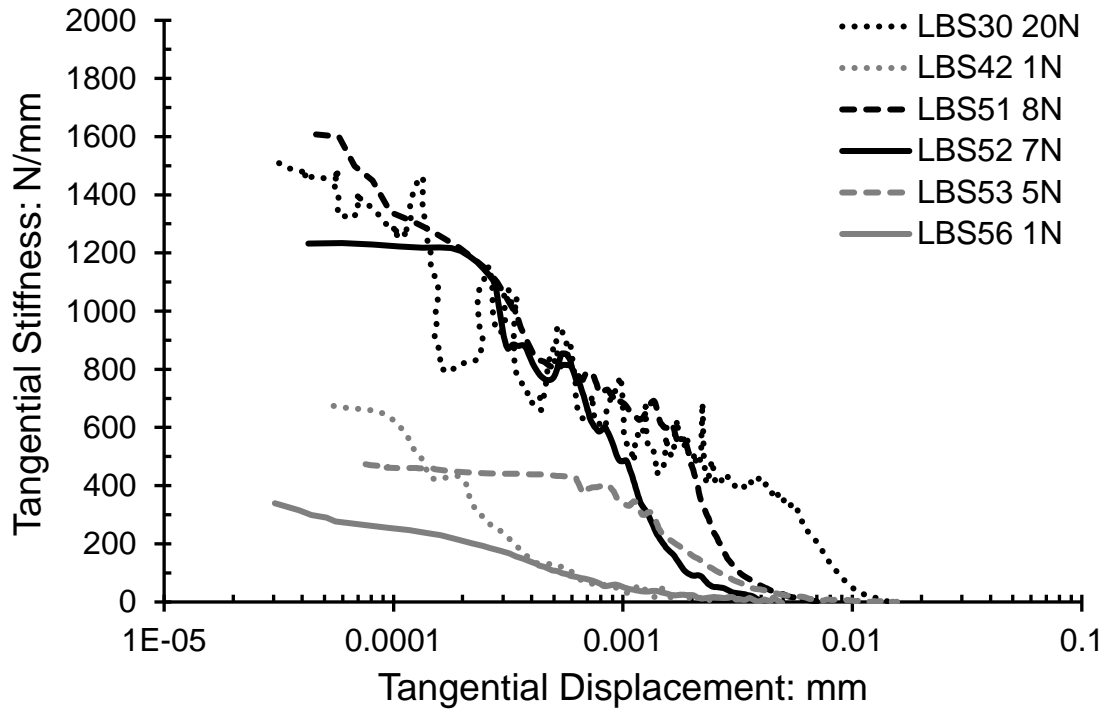
Fig. 8. Results in terms of force-displacement (a) and stiffness-displacement (b) of 6 tangential loading tests carried out on LBS particles with different normal forces under water immersed conditions.
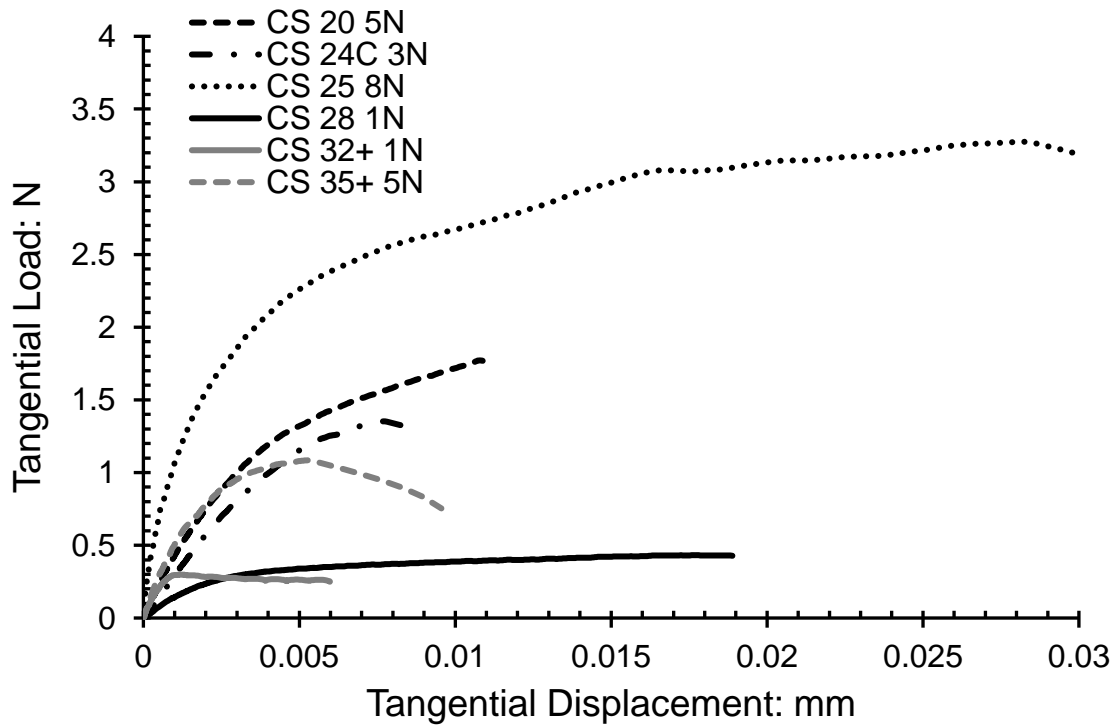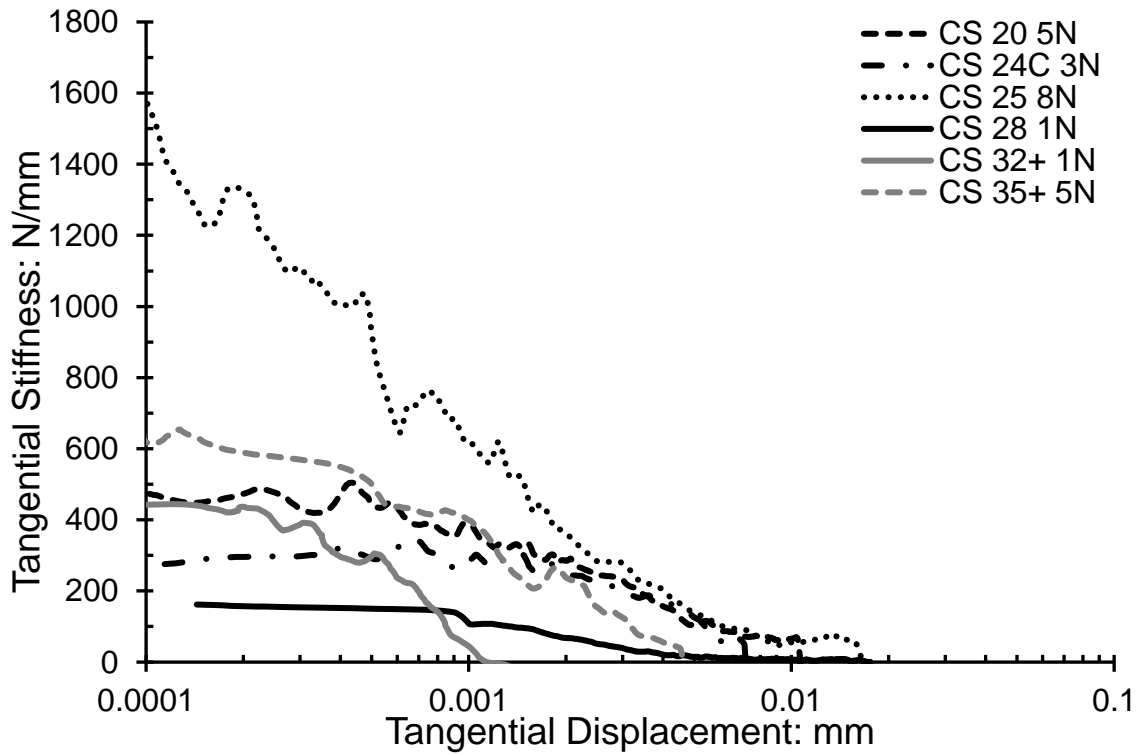
Fig. 9. Results in terms of force-displacement (a) and stiffness-displacement (b) of 6 tangential loading tests carried out on CS particles confined under different normal forces under water immersed conditions.
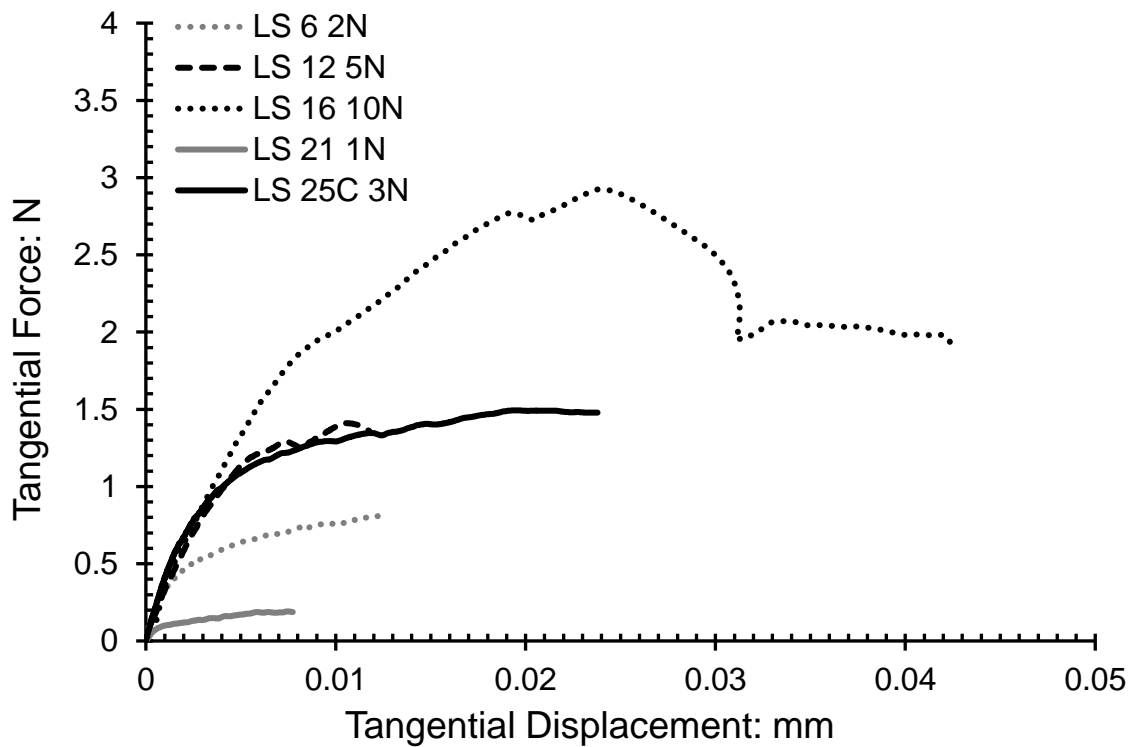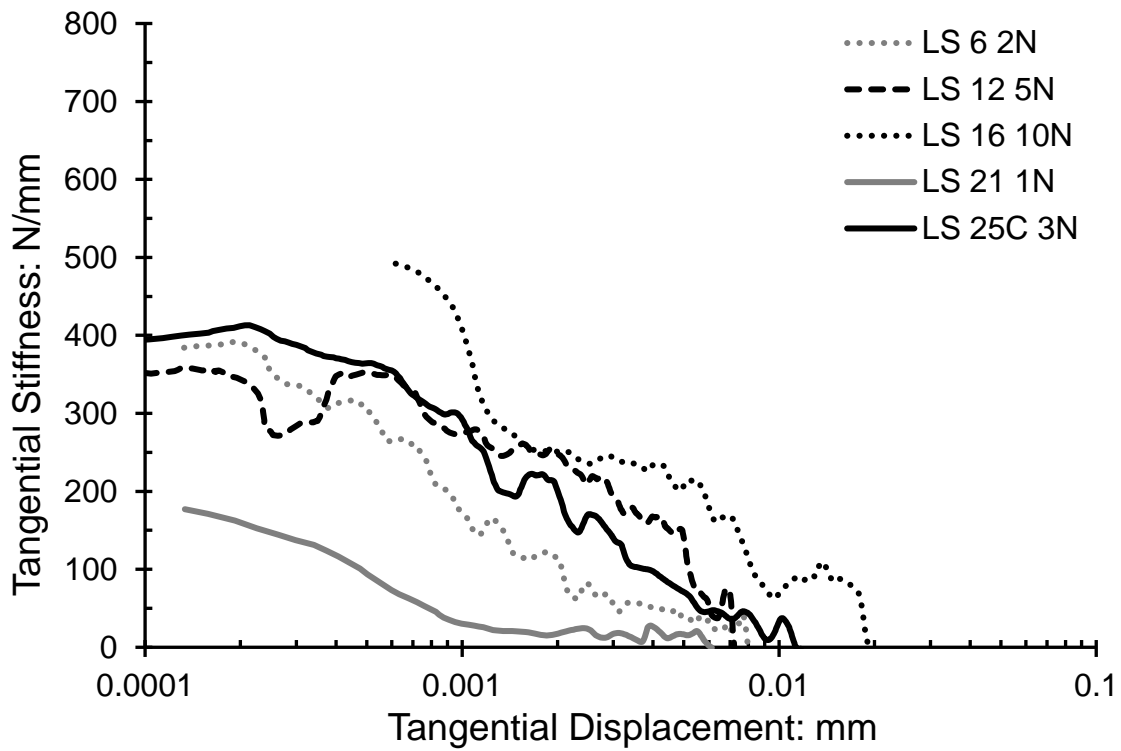
Fig. 10. Results in terms of force-displacement (a) and stiffness-displacement (b) of 5 tangential loading tests carried out on LS particles confined under different normal forces under water immersed conditions.
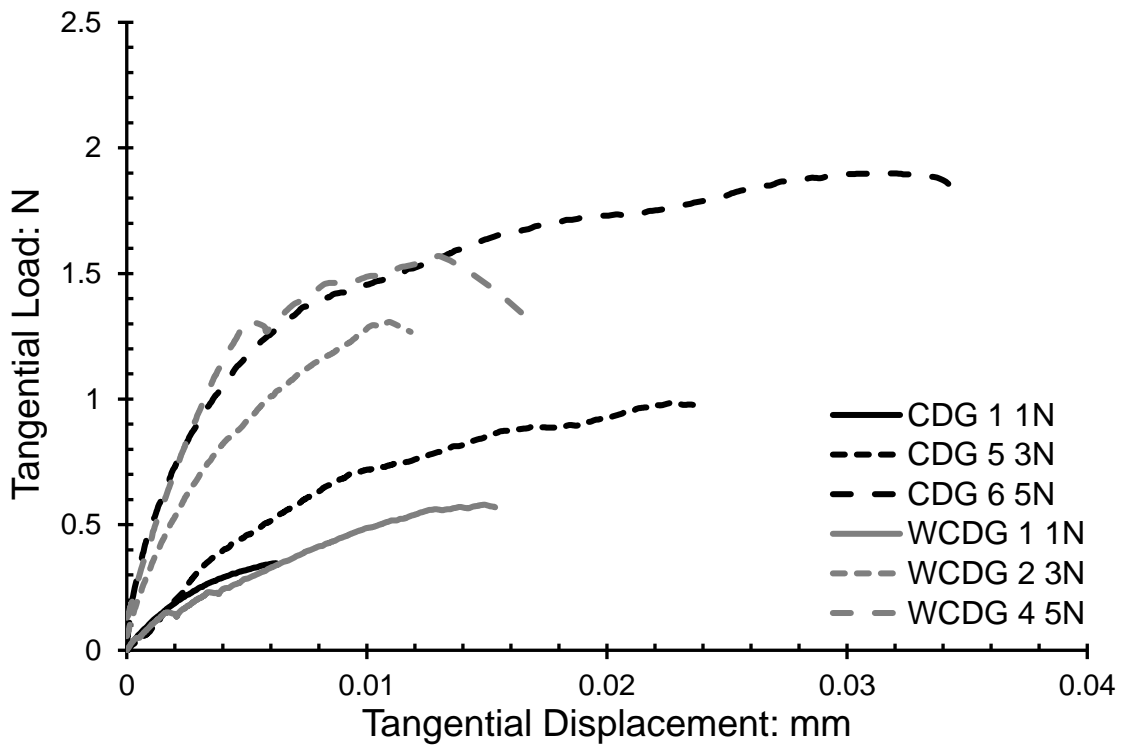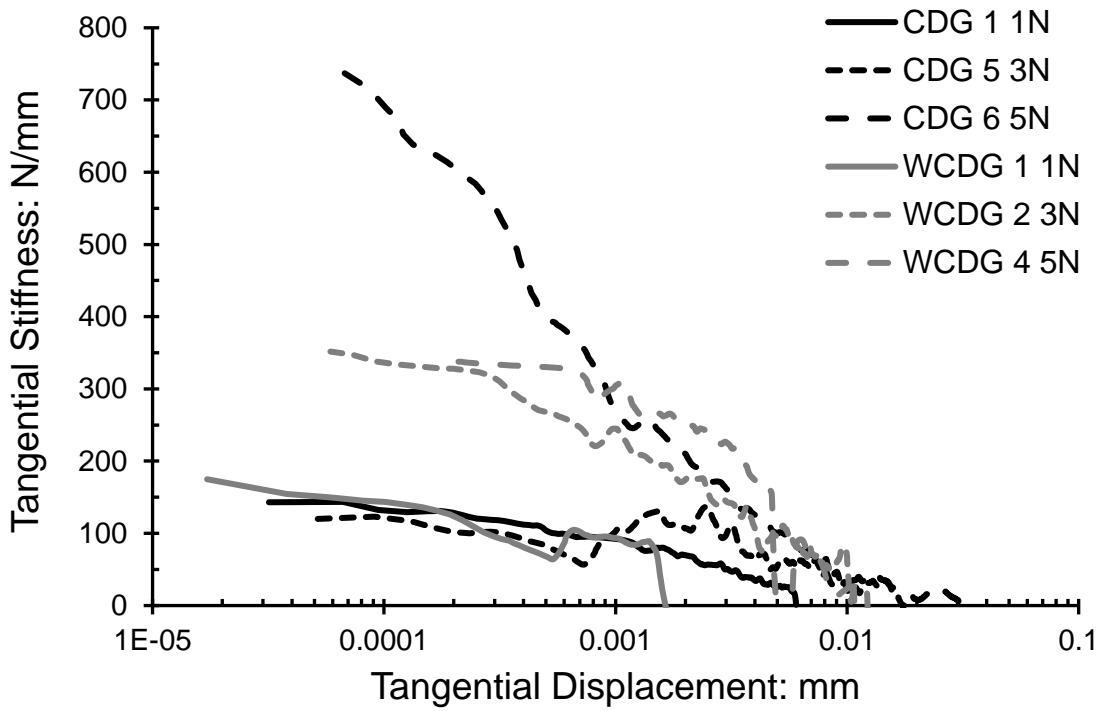
Fig. 11. Results in terms of force-displacement (a) and stiffness-displacement (b) of 3 tangential loading tests each carried out on CDG and WCDG particles confined under different normal forces.
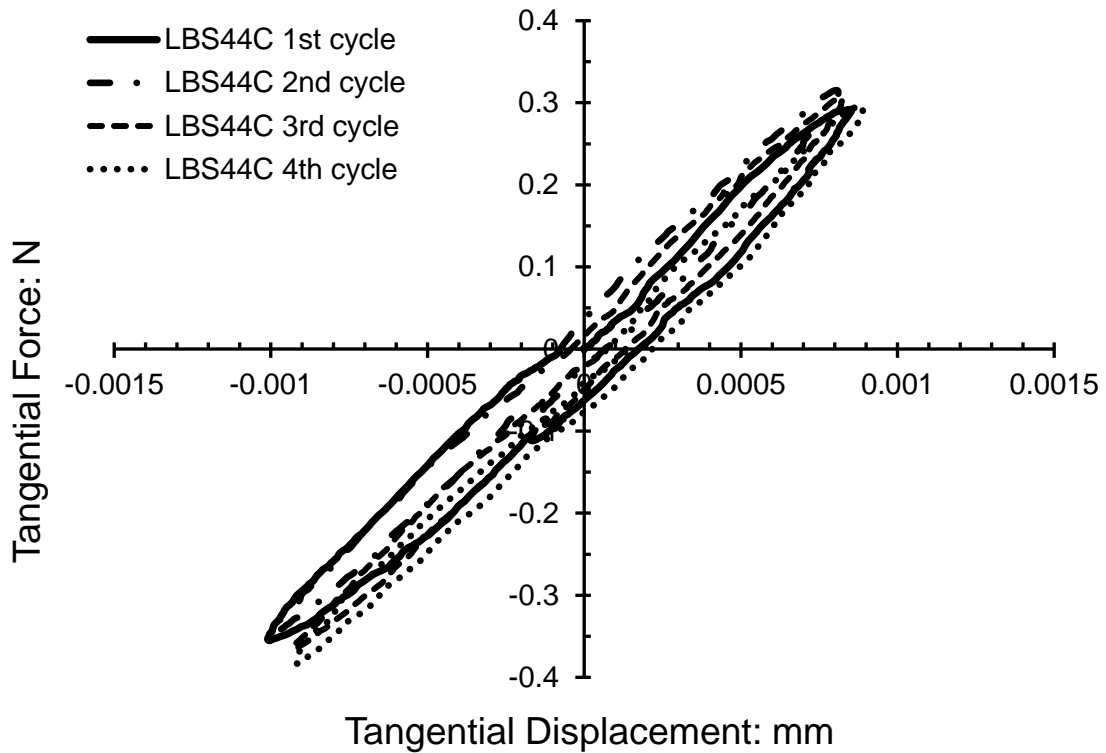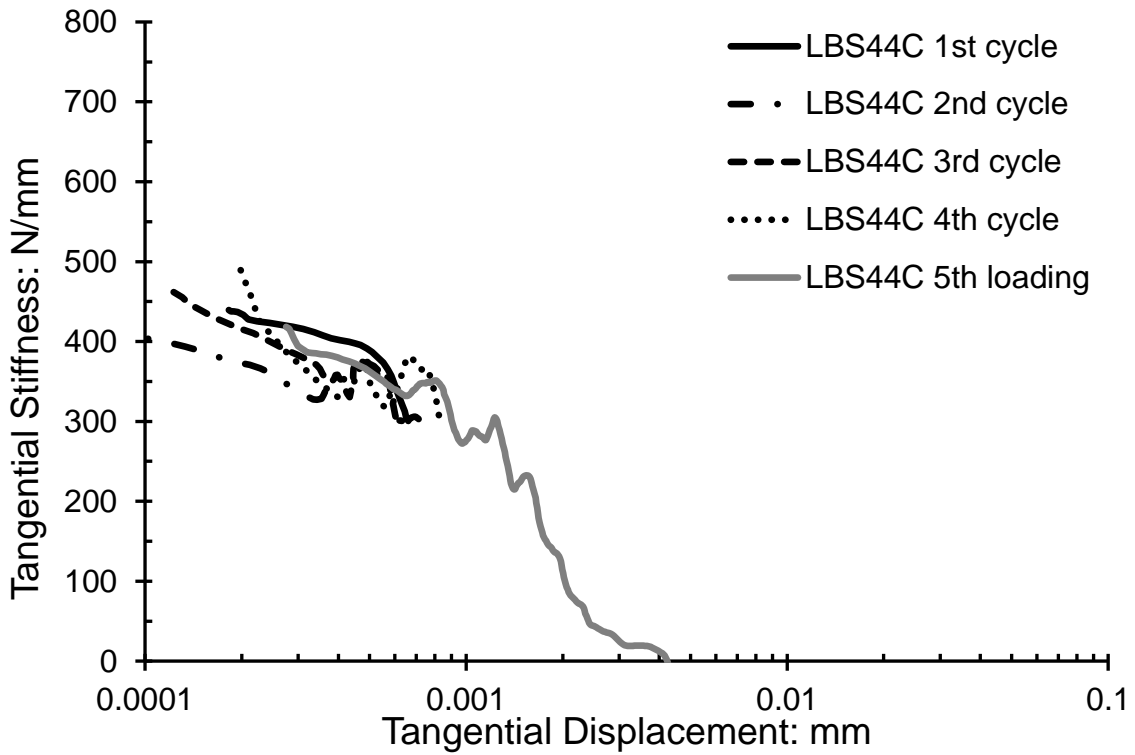
Fig. 12. Results of the cyclic tangential loading test LBSS44C in terms of force-displacement (a) and stiffness-displacement (b), where the particles were sheared over displacements of ±1μm and confined under 3N.
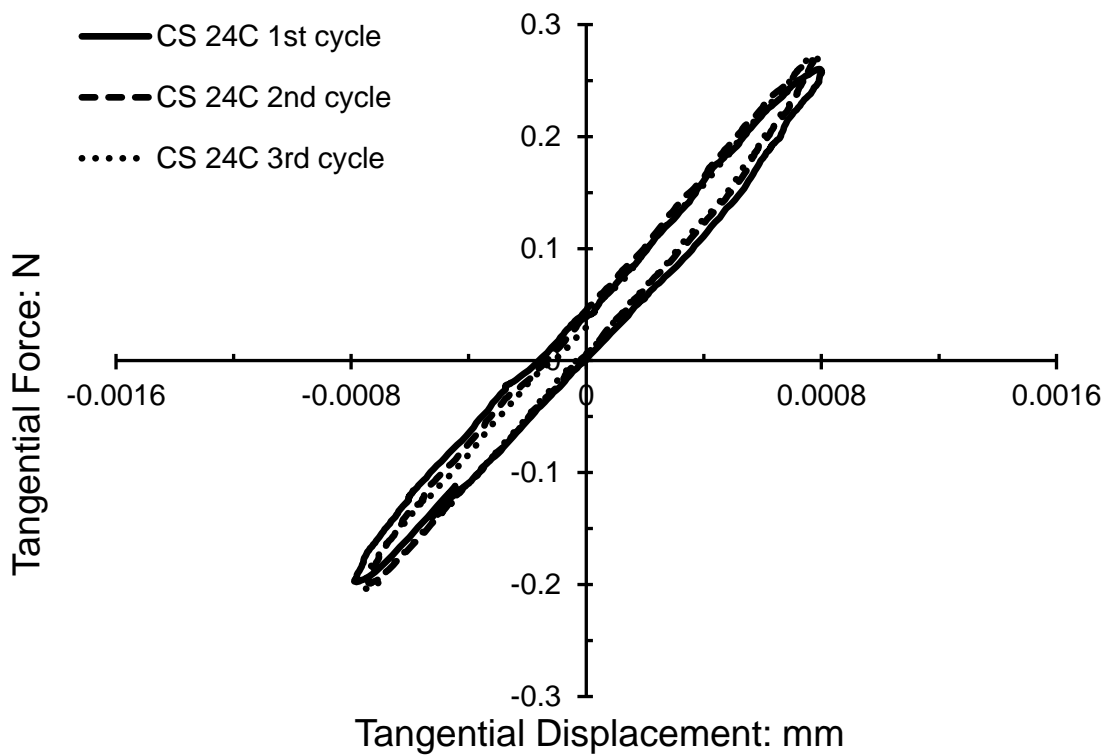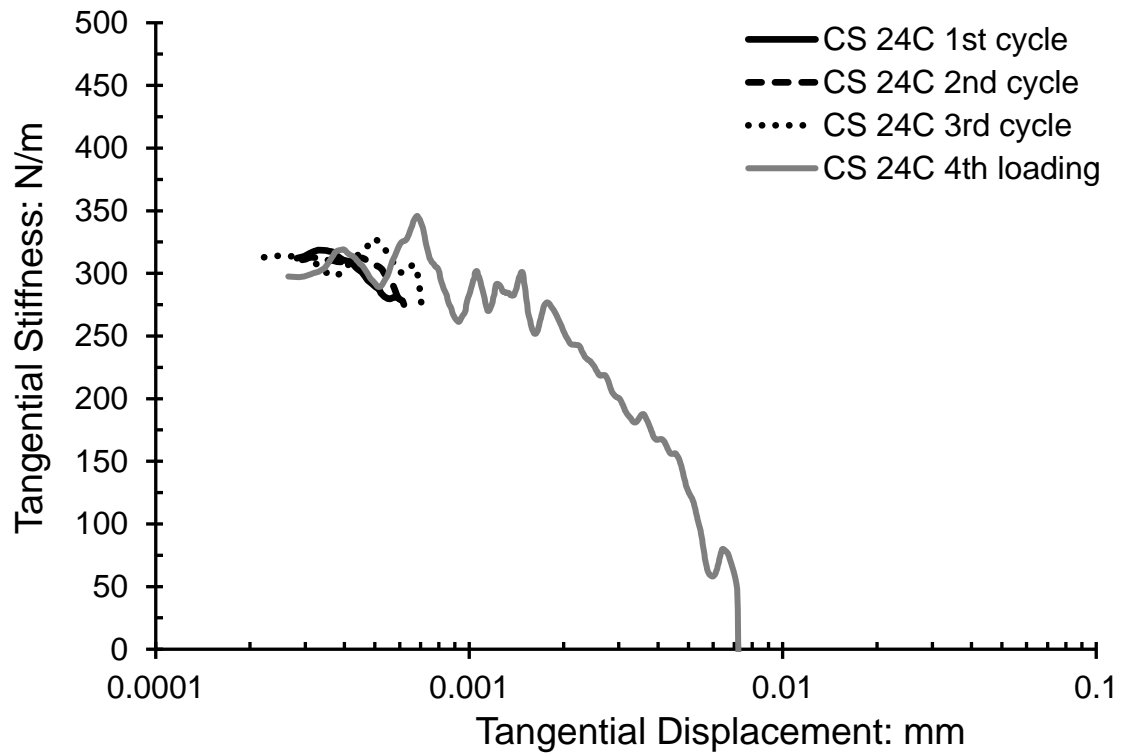
Fig. 13. Results of the cyclic tangential loading test CS24C in terms of force-displacement (a) and stiffness-displacement (b), where the particles were sheared over displacements of ±0.8μm and confined under 3N.

(a)

(b)
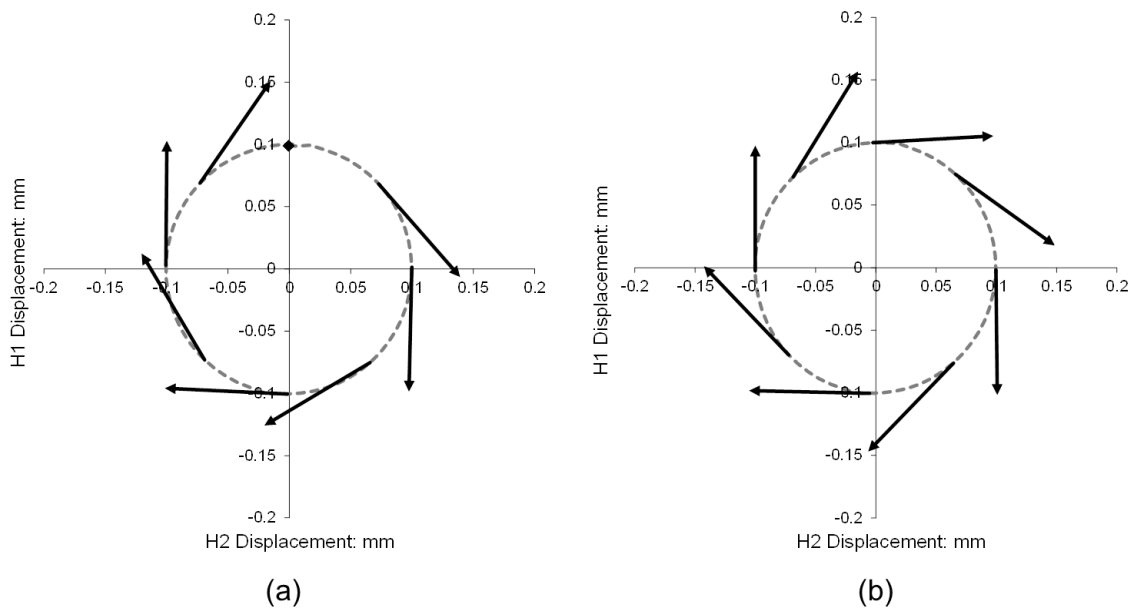
Fig. 14. Circular displacement paths and force increment vectors (black arrows) for the circular shearing test LBSC1: a) first cycle; b) twelfth cycle.
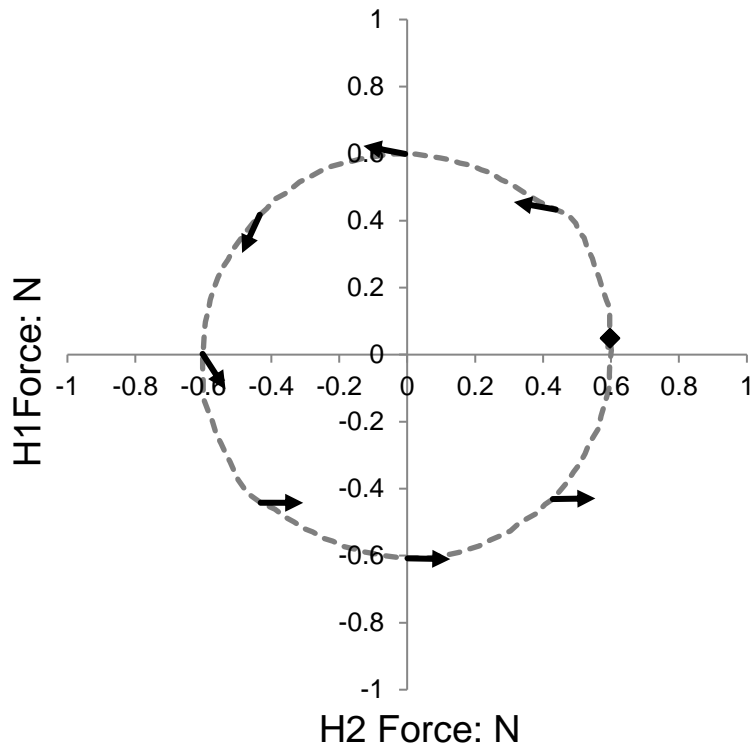
Fig. 15. Circular force path and displacement increment vectors (black arrows) plotted for a force-controlled circular shearing path.
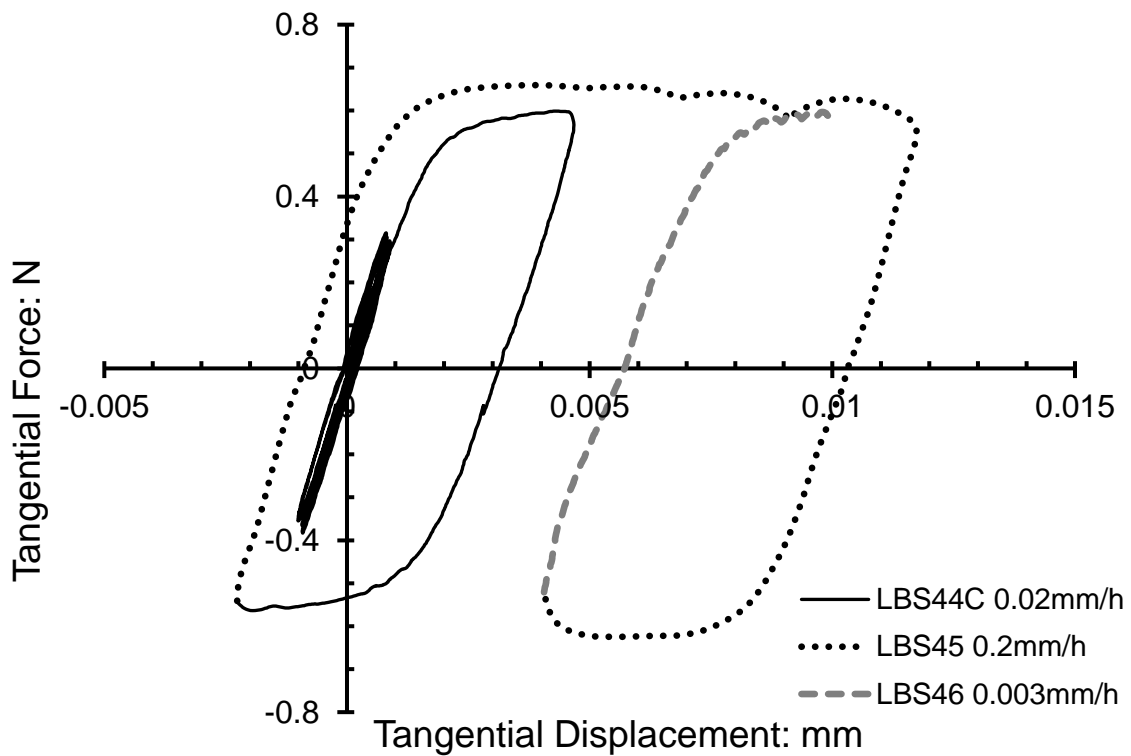
Fig. 16. Comparison of tangential loading tests performed on particles sheared at 0.02 mm/h (LBSS44C), 0.2mm/h (LBSS45) and 0.003mm/h (LBSS46) under a normal confinement of 3N.
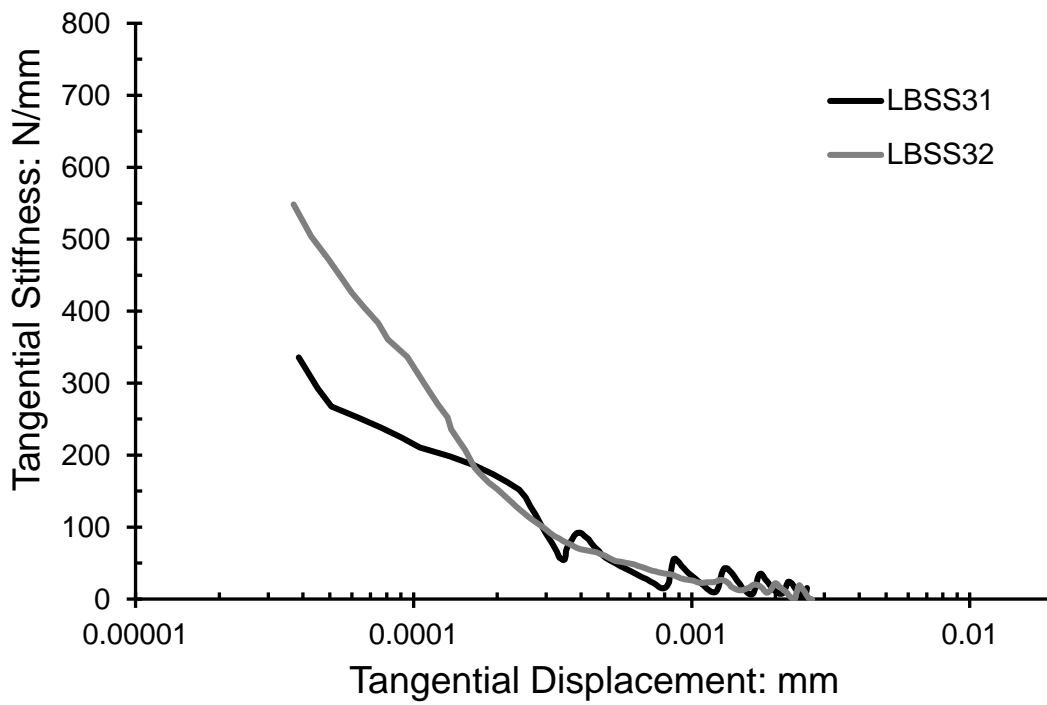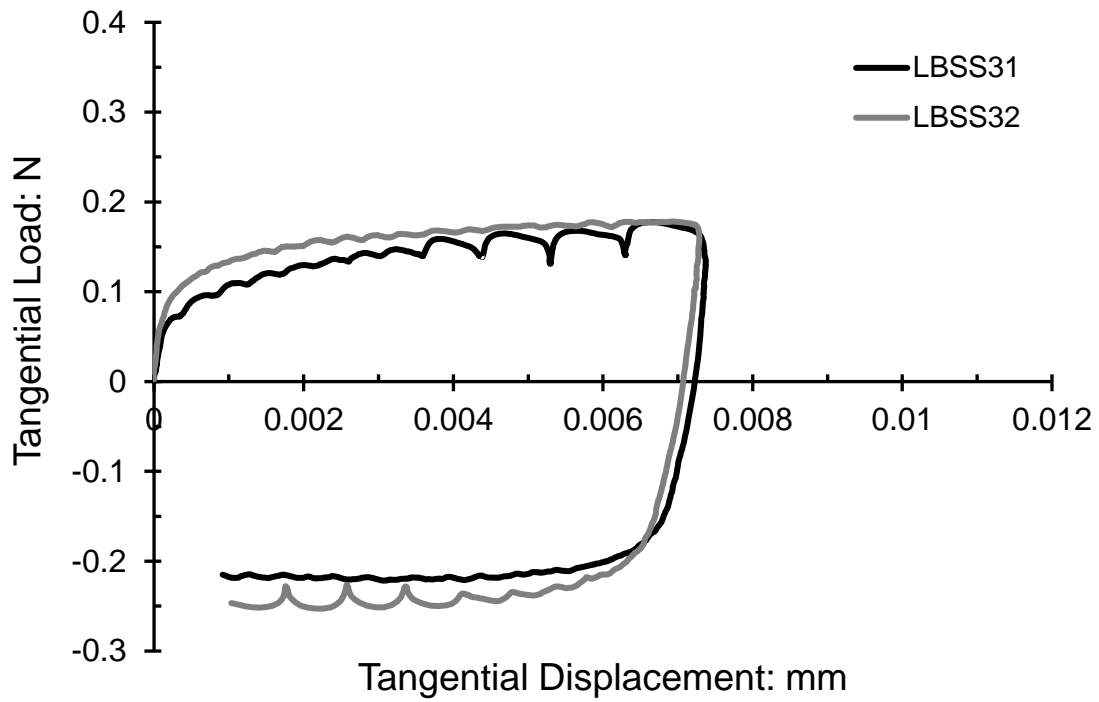
Fig. 17. Comparison in terms of force-displacement (a) and stiffness-displacement (b) between the results of a tangential loading tests on particles sheared at a normal load of 1N (LBSS31) and a similar test following compression of the same particles to 30N (LBSS32).
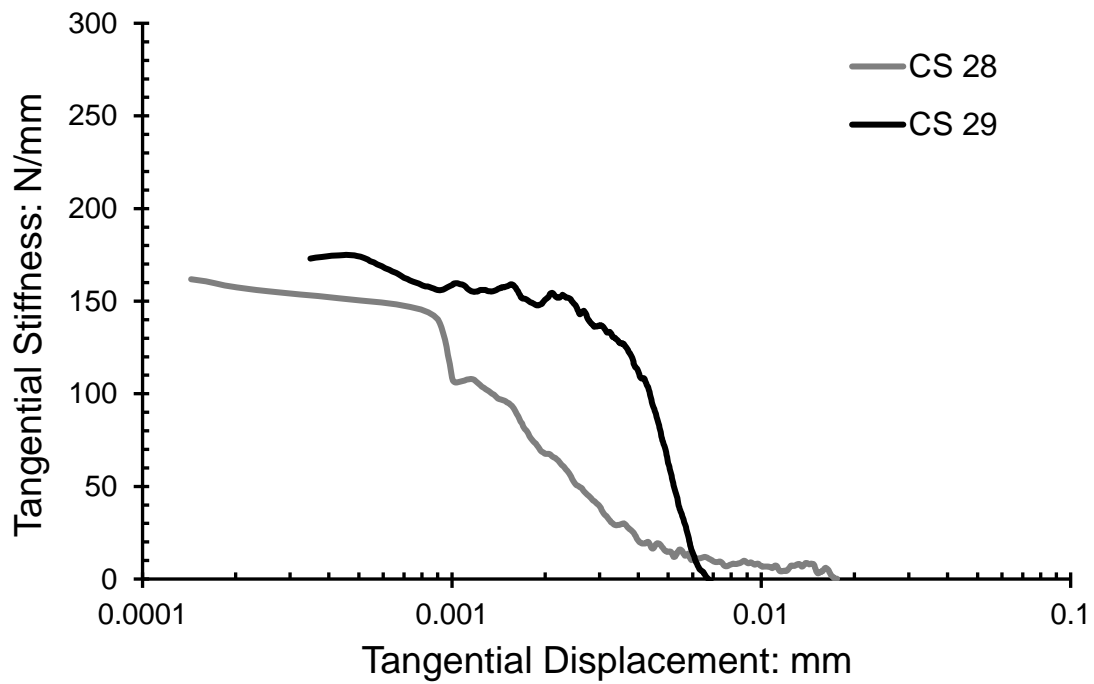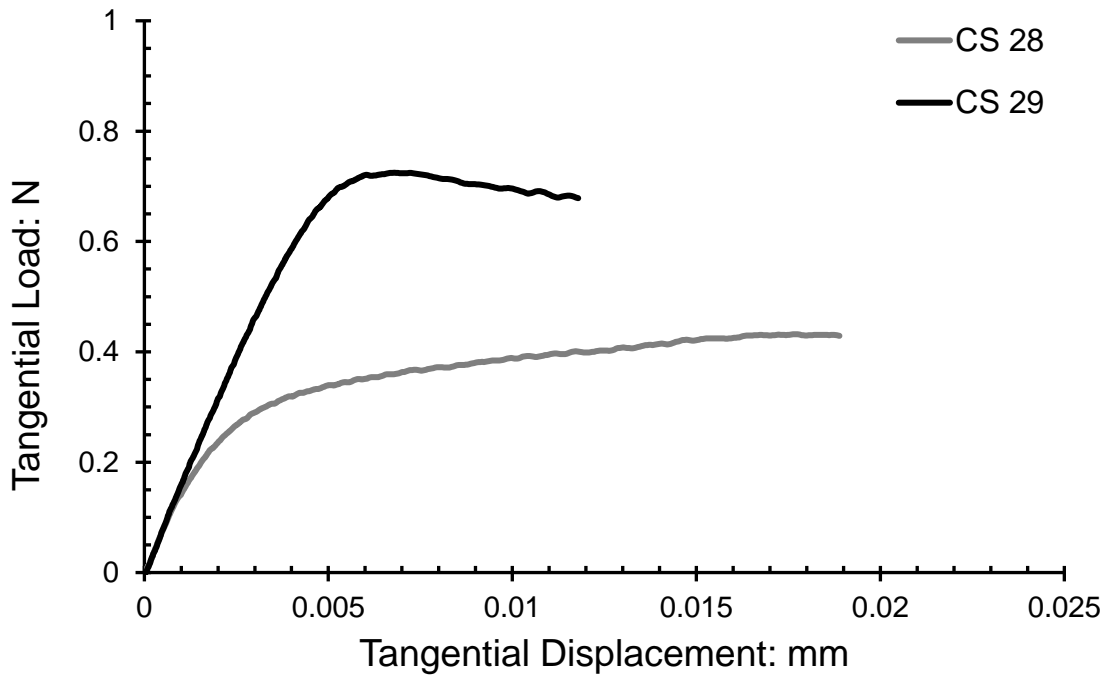
Fig. 18. Comparison in terms of force-displacement (a) and stiffness-displacement (b) between the results of a tangential loading test on particles sheared at a normal load of 1N (CS28) and a similar test on the same particles after compression to 10N (CS29).
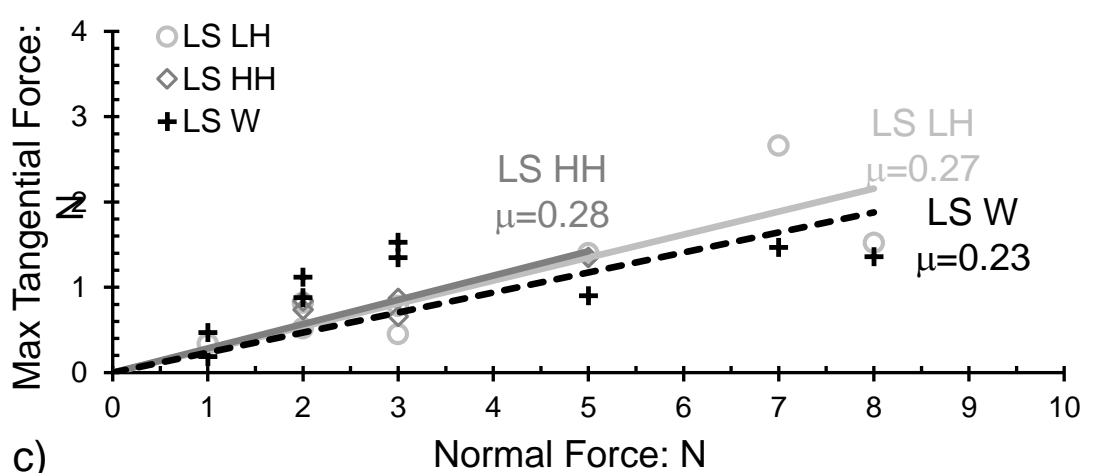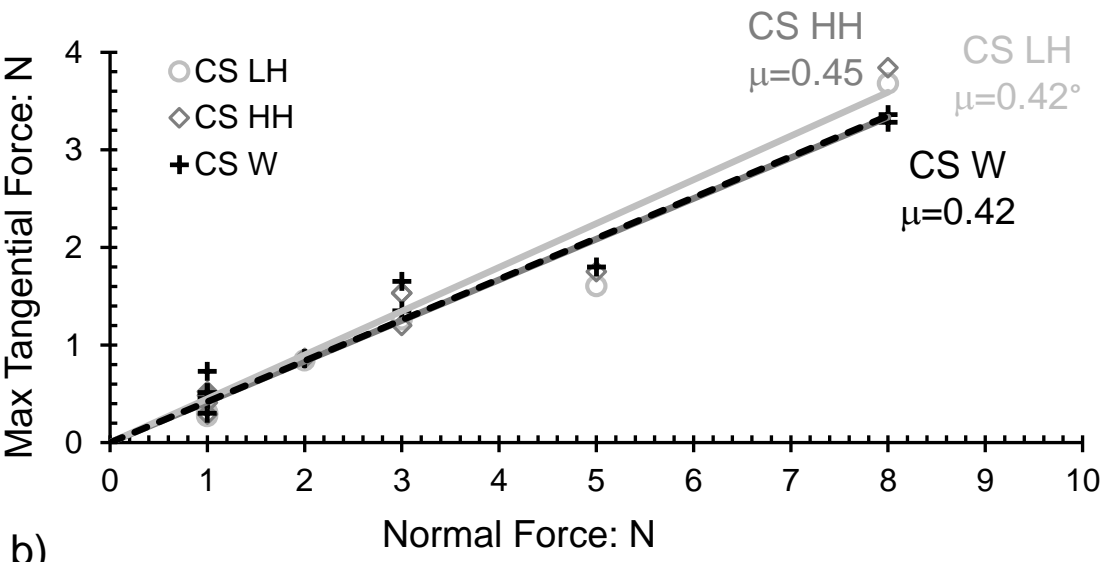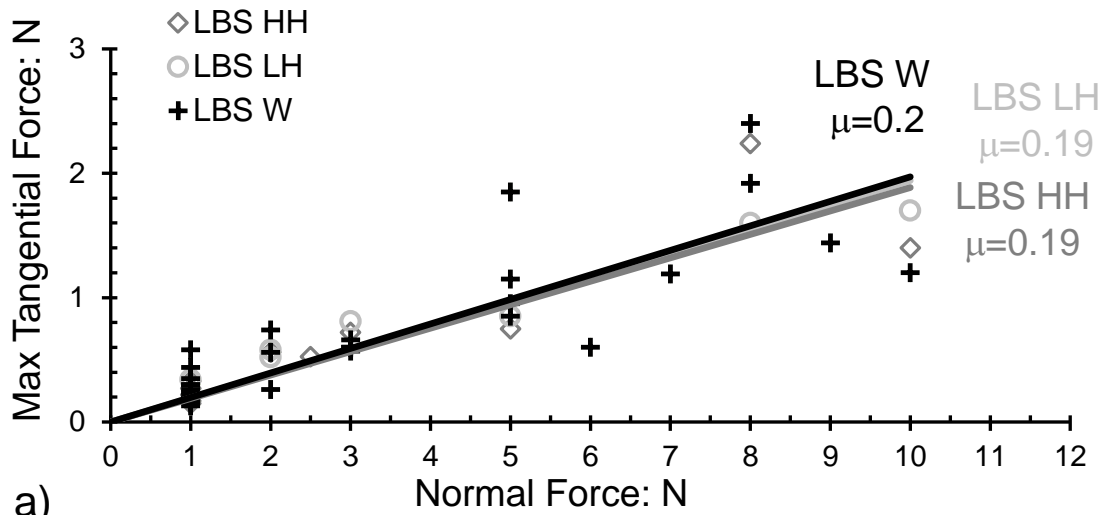
Fig. 19. Failure envelopes for LBS (a), CS (b) and LS (c) particles for different environmental conditions: LH: low humidity (RH≤30%); HH: high humidity (RH≥80%); W: water immersed.
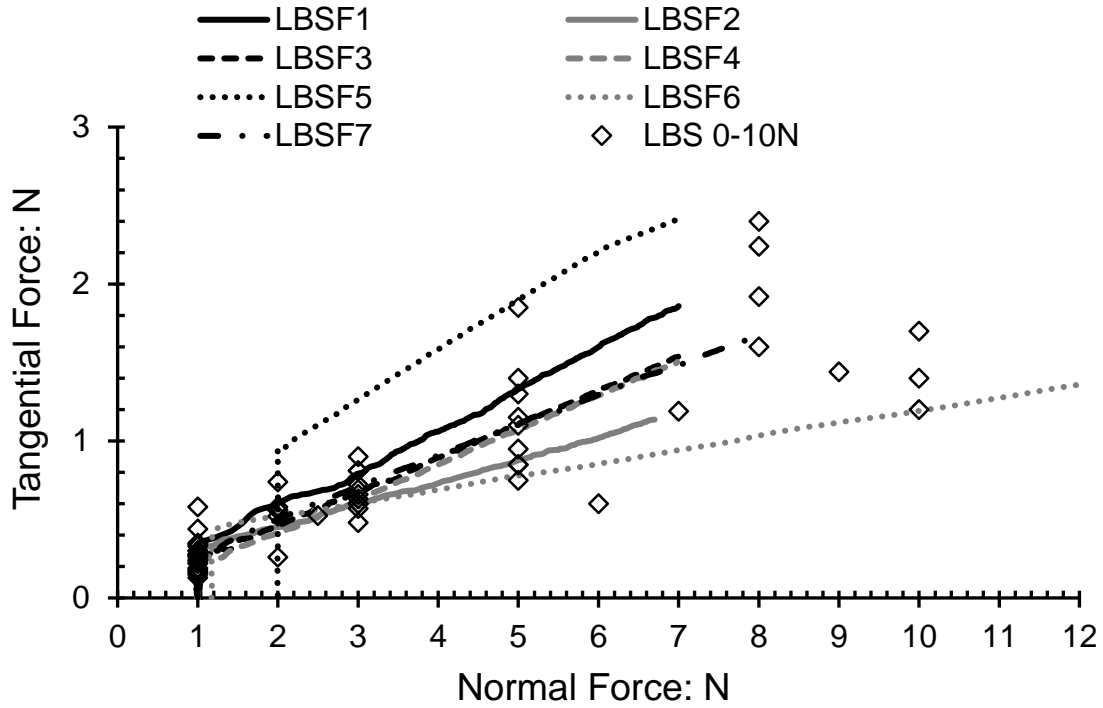
Fig. 20. Summary of all the tangential loading and friction tests carried out on LBS particles at lower normal loads.
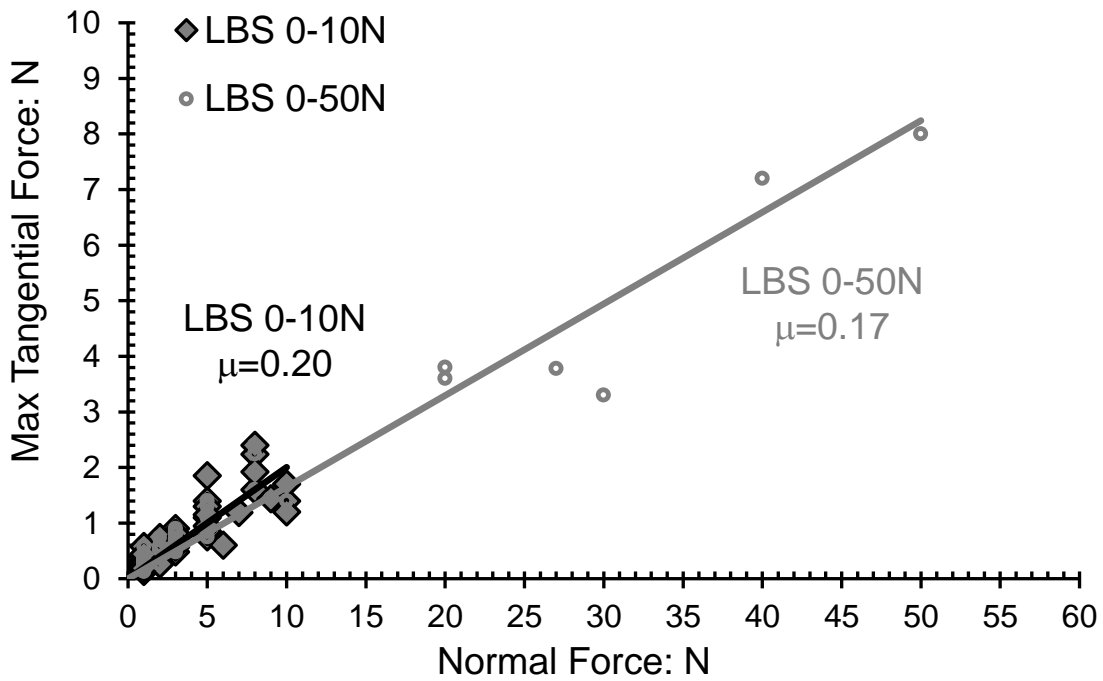

Fig. 21. Failure envelopes for LBS particles for different normal load levels (0-10N and 0-50N).
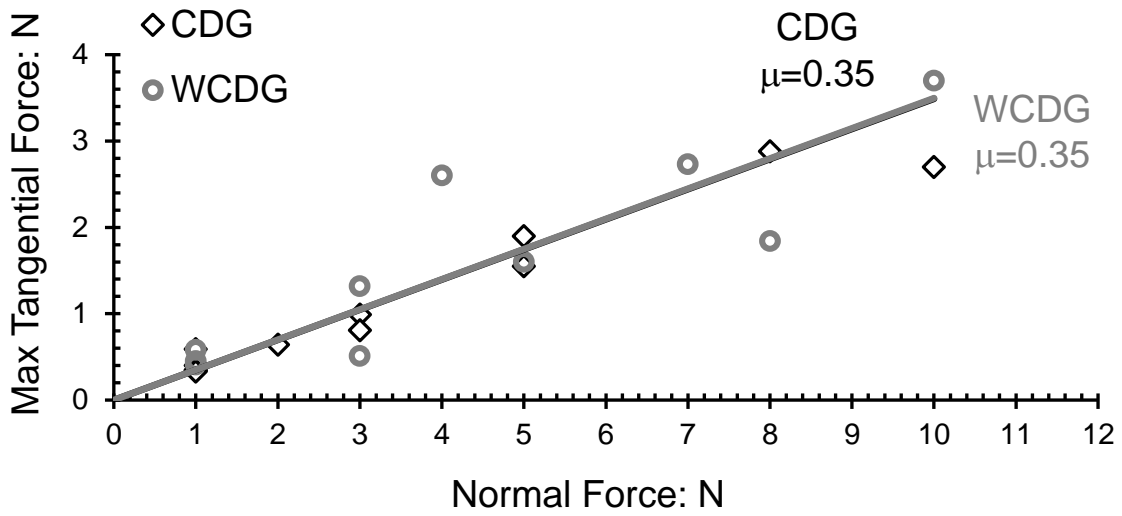
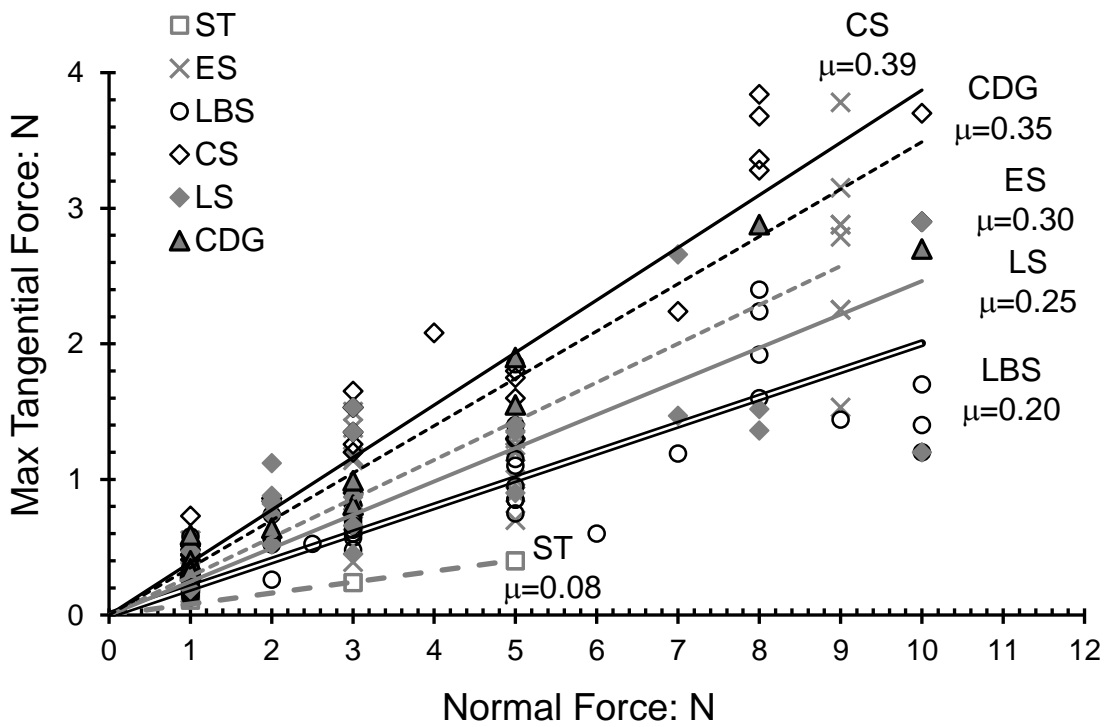Fig. 22. Failure envelopes for CDG and WCDG.

Fig. 23. Summary of the failure envelopes for all the sands tested along with chrome steel balls (ST) and Eglin sand (ES).
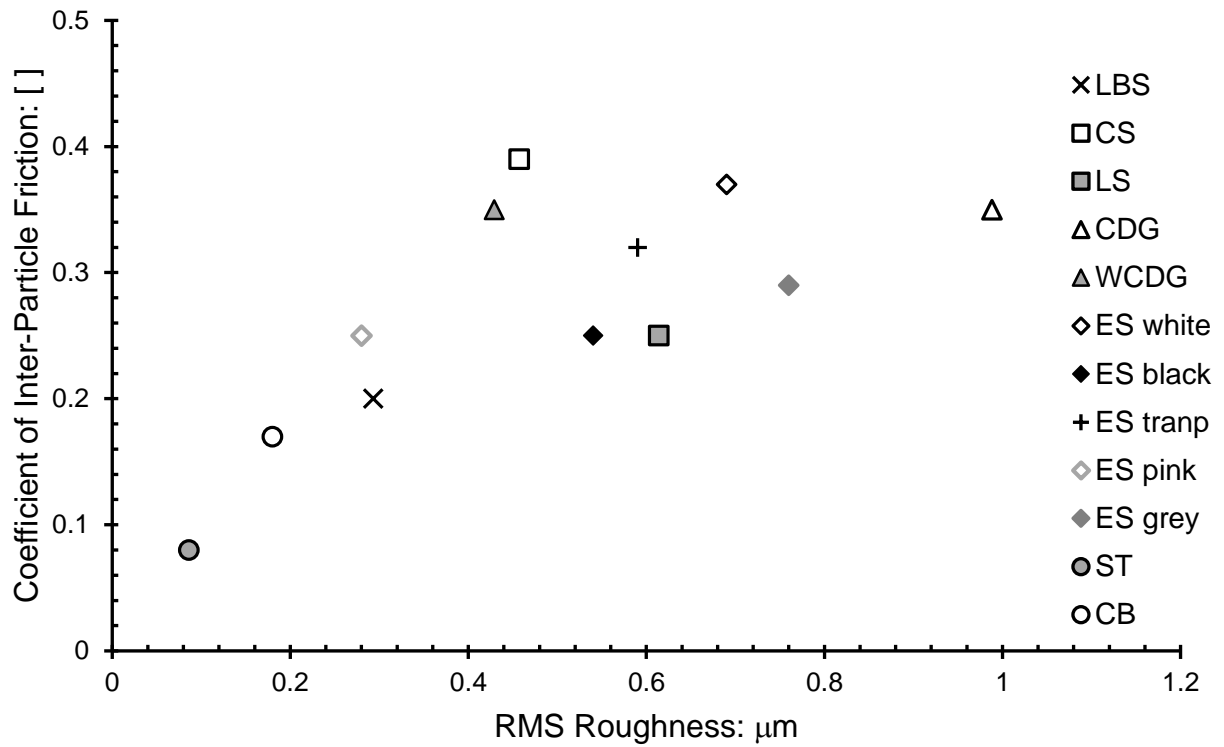
Fig. 24. Relationship between the average roughness of the materials tested and their average coefficients of inter-particle friction (ST: chrome steel balls, CB: ceramic balls).
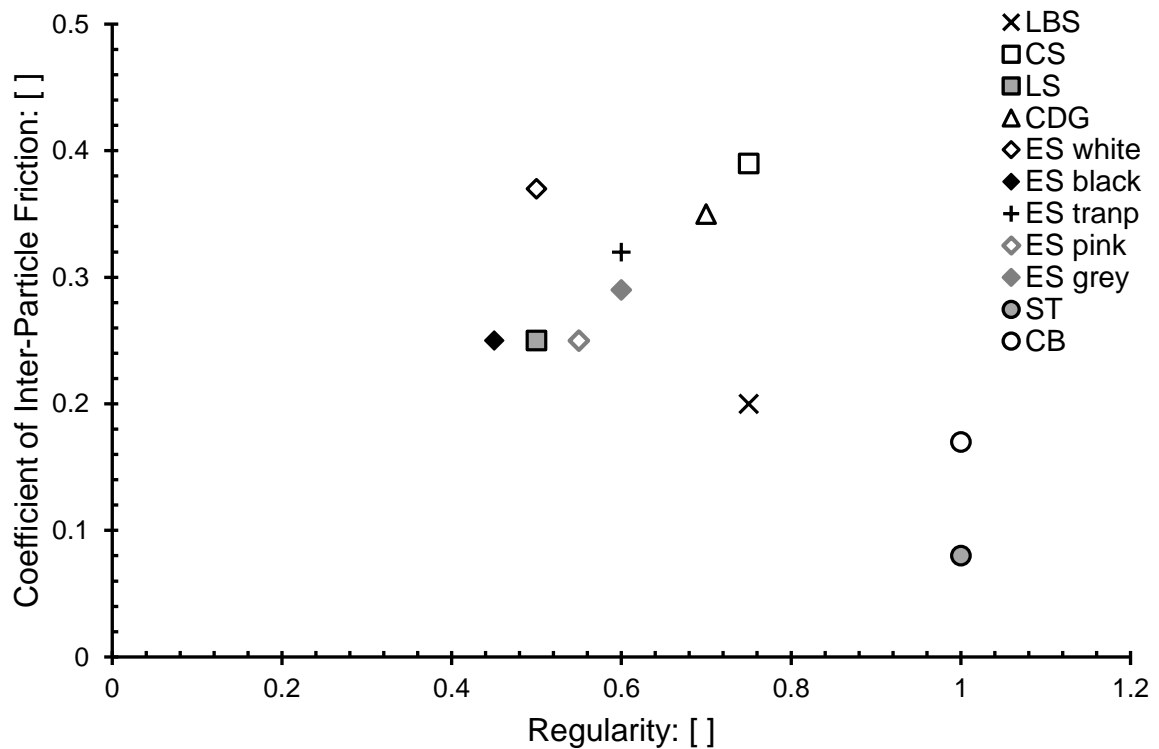

Fig. 25. Relationship between the average regularity of the particles tested and their average coefficients of inter-particle friction (ST: chrome steel balls, CB: ceramic balls).
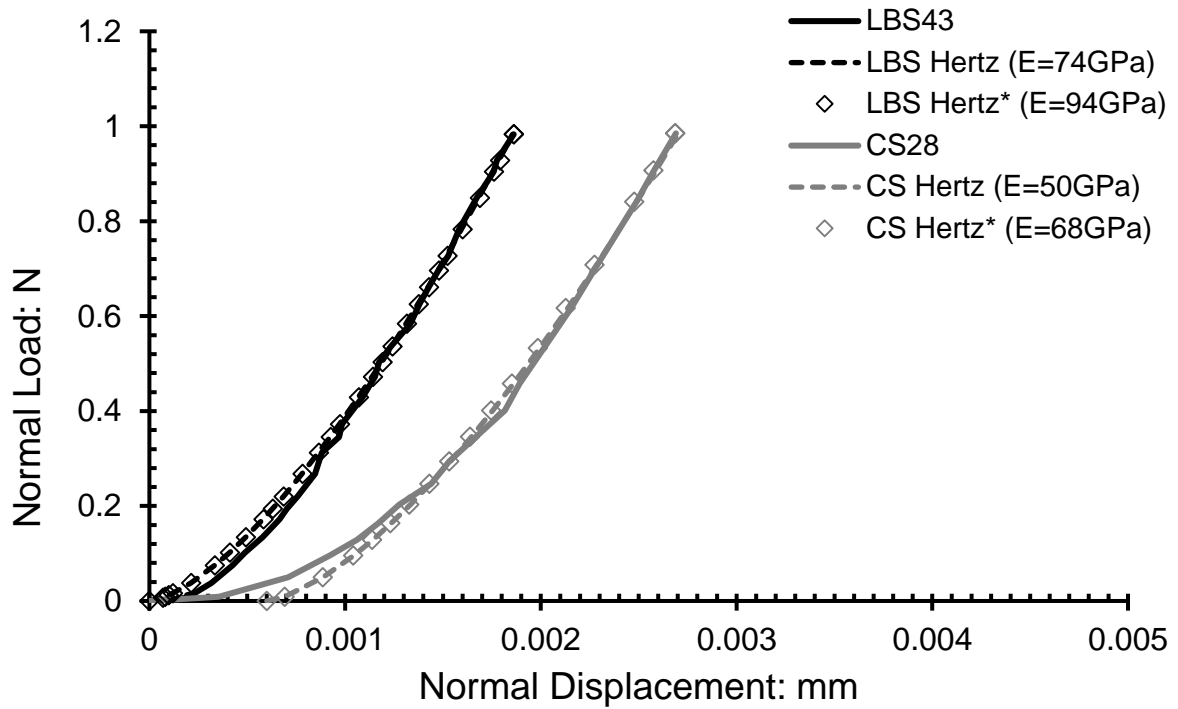
Fig. 26. Comparisons between normal loading tests LBS43 and CS28 up to 1N and the theoretical curves obtained from the classical Hertz theory (1882) and including surface roughness (*).
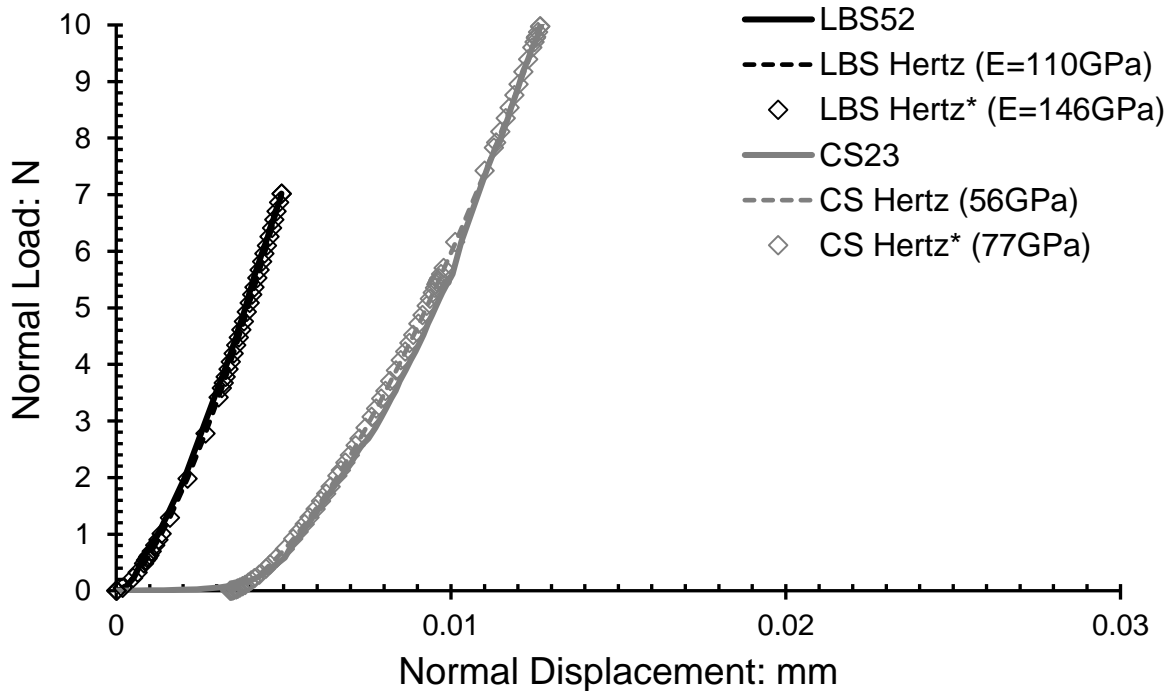

Fig. 27. Comparisons between normal loading tests LBS52 and CS23 up to 7 and 10N, and the theoretical curves obtained from the classical Hertz theory (1882) and including surface roughness (*).
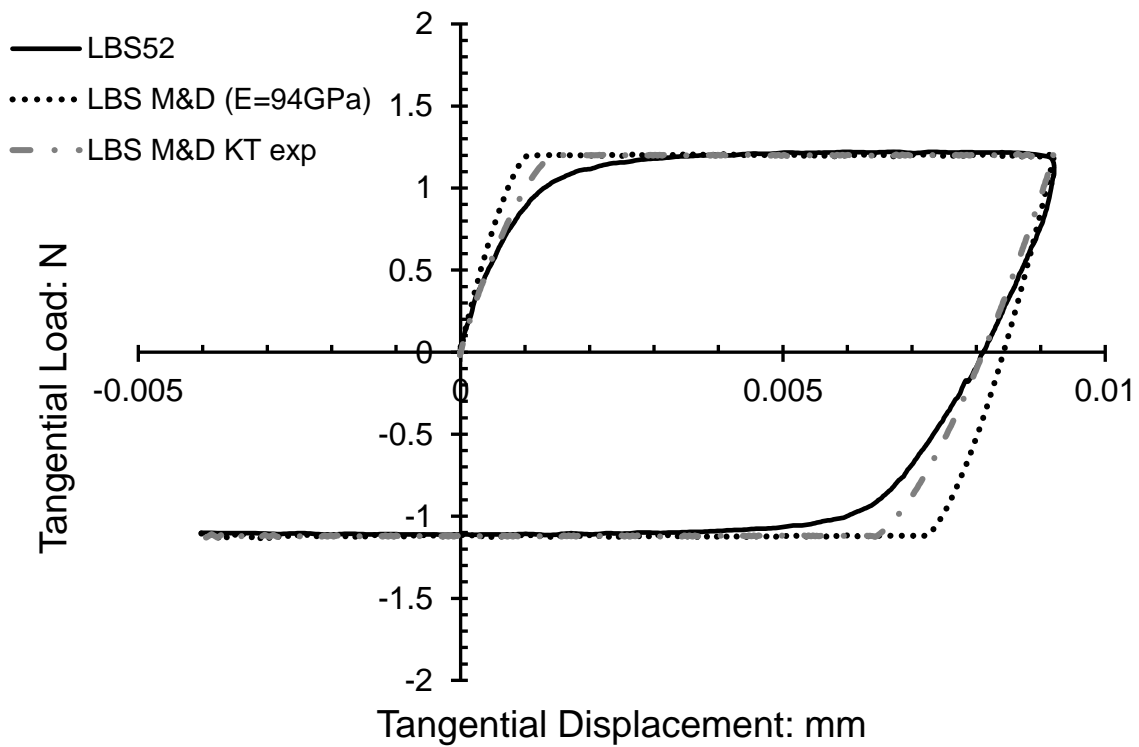
Fig. 28. Comparison between test LBSS52 and theoretical curves plotted using Mindlin & Deresiewicz (1953) using the calculated and measured initial stiffnesses.

Fig. 29. Comparison between the stiffnesses of LBS at 0.1 and 1μm and those predicted using Mindlin & Deresiewicz (1953) for the cases of small (D_{min} = 1.18mm) and large (D_{max} = 3.5mm) particle diameters.
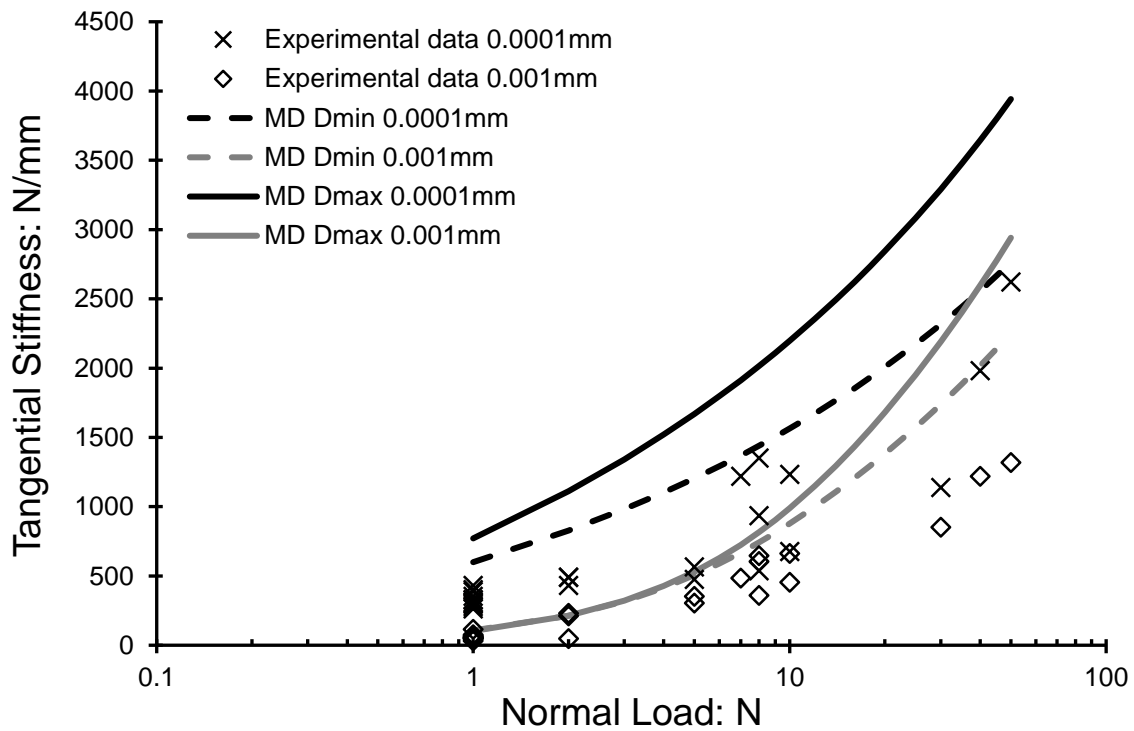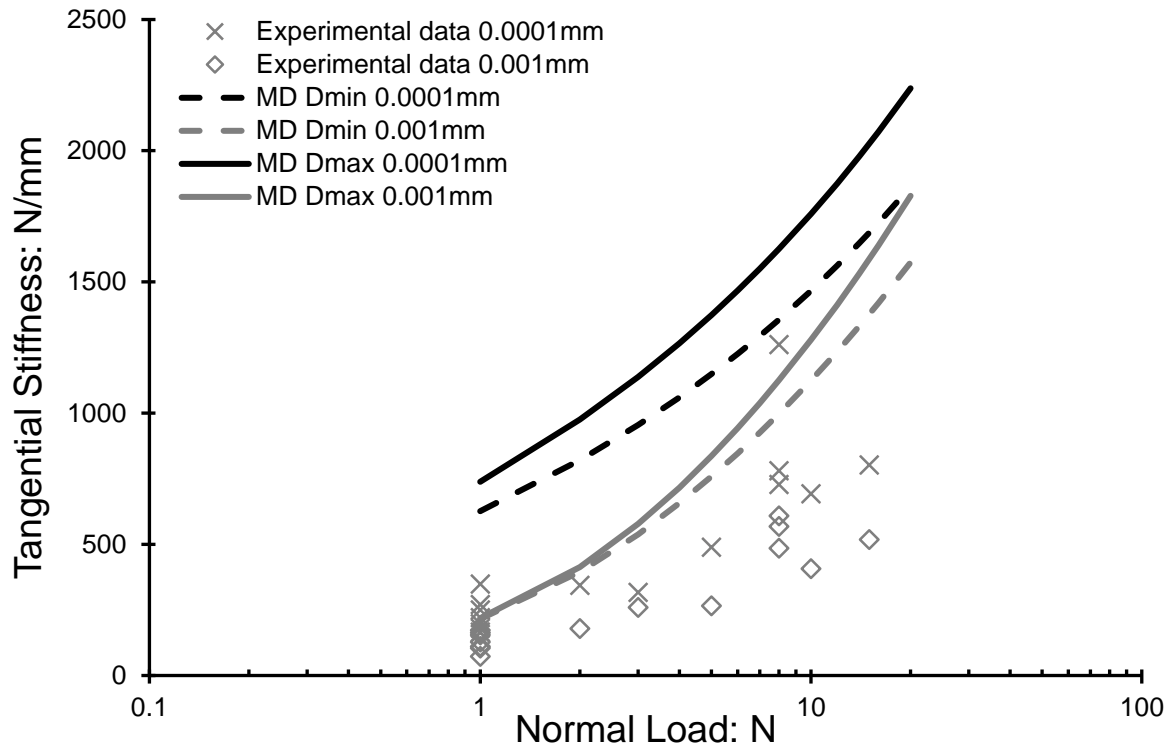
Fig. 30. Comparison between the stiffnesses of CS at 0.1 and 1μm and those predicted using Mindlin & Deresiewicz (1953) in cases of small (D_{min} = 2mm) and large (D_{max} = 3.5mm) particle diameters.

Table 1 – Chemical composition through EDS analyses of Leighton Buzzard sand (LBS), carbonate sand (CS), crushed limestone (LS) and completely decomposed granite (CDG).

	Sand type			
	LBS	CS	LS	CDG
Si (%)	49.0	0.6	-	24.7
O (%)	41.2	39.6	39.6	48.1
Al (%)	1.9	-	-	22.0
Fe (%)	7.5	-	-	3.2
K (%)	0.4	-	-	2.0
Na (%)	-	1.2	-	-
Cl (%)	-	0.4	-	-
Mg (%)	-	1.2	-	-
Ca (%)	-	37.9	40.6	-
C (%)	-	19.1	19.8	-

Table 2 – Particle shape and roughness characteristics.

Material	Size range (mm)	Roundness	Sphericity	RMS Roughness (μm)
Leighton Buzzard sand	1.18-2.36, 2.36-5	0.7	0.8	0.293 ± 0.087
Carbonate sand	2.36-5	0.7	0.7	0.457 ± 0.082
Limestone	2.36-5	0.3	0.7	0.614 ± 0.341
CDG	2.36-5	0.6	0.8	0.988 ± 0.303
Eglin sand[§]	1.18-2.36	0.4	0.6	0.528 ± 0.322
Ceramic balls	2.80-2.85	1	1	0.180 ± 0.034
Chrome steel balls	2.37	1	1	0.086 ± 0.025

[§]: data from Nardelli et al., 2017.

Table 3 – Mechanical characteristics of the materials.

Material	E (GPa)	G (GPa)	ν	Microhardness (GPa)	Indentation modulus E_I (GPa)
Leighton Buzzard sand	94-98[§]	44-46[§]	0.065-0.068[§]	6.0	104.8 124.0[¤] 117.6[¶]
Carbonate sand	73-84[§]	28-32[§]	0.30-0.32[§]	0.5	22.4 78.1[¶]
Limestone	73-84[§]	28-32[§]	0.30-0.32[§]	1.6 [†]	53.0[†] 78.1[¶]
CDG	-	-	-	0.4	7.2
Chrome steel balls	200	-	-	7.0	177.4

[§]: data from Mavko et al., 1998; Jaeger et al., 2007.
[¤]: values determined from nanohardness tests on quartz (Oliver and Pharr, 1992).
[¶]: values determined from nanohardness tests on quartz and calcite (Broz et al., 2006).
[†]: data from Todisco et al., 2017.

Table 4 – Summary of the shear tests carried out for each sand tested.

Material	Test type	Number of tests	Confining force (N)	Displacement rate (mm/h)
LBS	Tangential loading	65	1-50	0.003-0.2
	Friction	7	1-20	0.02-0.03
	Circular loading	5	1-4	0.3-0.6
CS	Tangential loading	38	1-15	0.02-0.05
LS	Tangential loading	25	1-10	0.02-0.06
CDG	Tangential loading	13	1-10	0.02-0.05
WCDG	Tangential loading	10	1-10	0.02-0.08